University of BRISTOL

High Mediterranean water-level during the Lago-Mare phase of the Messinian Salinity Crisis: insights from the Sr isotope records of Spanish marginal basins (SE Spain)

F. Andreetto [a,*], K. Matsubara [b], C.J. Beets [b], A.R. Fortuin [b], R. Flecker [c], W. Krijgsman [a]

[a] *Department of Earth Sciences, Utrecht University, Budapestlaan 17, 3584 CD Utrecht, the Netherlands*
[b] *Faculty of Earth and Life Sciences, Vrije Universiteit, De Boelelaan 1085, 1081HV Amsterdam, the Netherlands*
[c] *BRIDGE, School of Geographical Sciences and Cabot Institute, University of Bristol, University Road, Bristol BS8 1SS, UK*

ABSTRACT

The Messinian Salinity Crisis (MSC) successions record extreme fluctuations in the Mediterranean's environmental conditions. However, some of the scenarios that are thought to have caused these extreme environments are contentious. One prominent example of this is the Mediterranean water level during the Lago-Mare stage of the MSC, which is interpreted either as being very low during a largely desiccated Mediterranean punctuated by endorheic lakes (lacustrine scenario) or sufficiently high to enable basin-wide connectivity across the Mediterranean and with the Atlantic and the Eastern Paratethys (lagoonal scenario). In SE Spain, adjoining marginal basins of Sorbas, Nijar and Vera exhibit sedimentary records of the Lago-Mare stage. Here we present 11 new $^{87}Sr/^{86}Sr$ isotope ratios measured on ostracod (*Cyprideis* sp.) valves from these successions, which add to the 11 already published data from these basins and whose significance, in terms of water provenance, has not been fully explored. In parallel, we construct a mass balance model that provides quantitative insights into the Sr isotopic composition of the water in which the ostracods dwelt. Overall, measured and published $^{87}Sr/^{86}Sr$ isotope ratios from Sorbas (0.709066–0.709131), Nijar (0.708814–0.709099) and Vera (0.708764–0.708813) all show lower values than modelled ratios for endorheic lakes (>0.7100). These Spanish basins therefore require an additional source of water with a lower Sr isotope signature which is likely to have been derived from the main Mediterranean waterbody (0.7086–0.7087). This interpretation implies that at least the Western Mediterranean had a relatively high and fluctuating water level during the Lago-Mare stage of the MSC.

1. Introduction

Late Messinian hydrological changes in the Mediterranean, instigated by reduced connectivity with the Atlantic Ocean (Flecker et al., 2015; Krijgsman et al., 2018) and increased connectivity with the Eastern Paratethys (Flecker and Ellam, 2006; Krijgsman et al., 2010; Grothe et al., 2020), are considered to have been the main cause of the ecological and environmental extremes experienced by the Mediterranean during the Messinian Salinity Crisis (MSC, Roveri et al., 2014a). Stage 1 (5.97–5.60 Ma) of the consensus chronostratigraphic model (Roveri et al., 2014a) is documented in onshore sedimentary records by successions of alternating primary gypsum-shales and marls-shales couplets (Primary Lower Gypsum, PLG; e.g., Lu, 2006; Lugli et al., 2010; Dela Pierre et al., 2011). Following a period (MSC Stage 2; 5.60–5.55 Ma) of extensive subaerial erosion (Hsü et al., 1973; Lofi et al., 2005) and salt deposition (Lugli et al., 1999), a second unit (Upper Gypsum, UG) of alternating gypsum and marls was deposited in the central (Sicily, Ionian Islands) and eastern regions (Crete, Cyprus) of the Mediterranean (MSC substage 3.1; 5.55–5.42 Ma; Manzi et al., 2009b, 2016). Multi-disciplinary observations relating to Mediterranean-Atlantic connectivity suggest that a persistent Atlantic inflow to the Mediterranean with restricted outflow is likely to have existed during PLG deposition (Hardie and Lowenstein, 2004; Lu, 2006; Krijgsman and Meijer, 2008; Lugli et al., 2007, 2010, 2013, 2015; Dela Pierre et al., 2011; Roveri et al., 2014a, 2014b; Flecker et al., 2015; García-Veigas et al., 2018; Manzi et al., 2018; Reghizzi et al., 2018), while a one-way flow with blocked outflow prevailed during halite and UG precipitation (Krijgsman and Meijer, 2008; Roveri et al., 2014c; Marzocchi et al.,

---

2016; Krijgsman et al., 2018). According to the consensus model of Roveri et al. (2014a), this connectivity configuration translated into a Mediterranean base-level at Atlantic level during PLG deposition and below during halite precipitation, even though halite precipitation in a full Mediterranean cannot be rule out (Krijgsman and Meijer, 2008; Roveri et al., 2014c; Meilijson et al., 2019). However, the connectivity history and water level of the Mediterranean during the final MSC phase, the Lago-Mare (or substage 3.2; 5.42–5.33 Ma), remain highly contested (see Orszag-Sperber, 2006; Roveri et al., 2014a; Caruso et al., 2019).

Rocks of this terminal MSC interval comprise mainly coarse- to fine-grained siliciclastic deposits (e.g., Roveri et al., 1998; Rouchy et al., 2001; Guerra-Merchán et al., 2010; Dela Pierre et al., 2011) and sporadic primary gypsum beds (Tuscany and Sicily, Italy; Roveri et al., 2008a; Manzi et al., 2009b). The sedimentary successions are frequently stacked in cycles interpreted to be precession driven (Fortuin and Krijgsman, 2003; Roveri et al., 2008a; Manzi et al., 2009b, 2016; Omodeo Salé et al., 2012). The fine-grained interbeds contain faunal assemblages that include brackish mollusks, ostracods and dinoflagellate cysts typical of the Black Sea region (Gliozzi et al., 2007; Stoica et al., 2016; Grothe et al., 2018; Sciuto et al., 2018). Such anomalohaline faunal associations have been recognized throughout the Mediterranean in both marginal settings (Malaga, Sorbas, Nijar and Vera basins in SE Spain, Piedmont Basin, Northern Apennines and Sicily in Italy, Crete, Cyprus and S Turkey) and in deep-sea records (DSDP 129A, 375, 376 and ODP 967, 968, 975, 978) (Roep and Van Harten, 1979; Cita et al., 1978; McCulloch and De Deckker, 1989; Blanc-Valleron et al., 1998; Spezzaferri et al., 1998; Bonaduce and Sgarrella, 1999; Iaccarino and Bossio, 1999; Rouchy et al., 2001; Bassetti et al., 2006; Cosentino et al., 2007; Grossi et al., 2008, 2015; Guerra-Merchán et al., 2010; Dela Pierre et al., 2011; Stoica et al., 2016).

The traditional view of Mediterranean paleogeography during the Lago-Mare phase is an isolated and desiccated Mediterranean studded with low-salinity endorheic lakes supplied with sediments and dissolved elements by local rivers (e.g., Ruggieri, 1967; Hsü et al., 1973; Cita et al., 1978; Orszag-Sperber et al., 2000; Ryan, 2009; Lymer et al., 2018; Camerlenghi et al., 2019; Caruso et al., 2019; Kartveit et al., 2019; Madof et al., 2019; Raad et al., 2020). In this scenario, the Black Sea ostracods, mollusks and dinoflagellates are considered to be transported by migratory aquatic birds (Benson, 1978; Benson and Rakic-El Bied, 1991; Caruso et al., 2019). Although it is not explicitly stated, the same scenario is endorsed by the proponents of the Zanclean flood as the mechanism that led to the replenishment of a desiccated Mediterranean (e.g., Amadori et al., 2018; Micallef et al., 2018, 2019; Ben-Moshe et al., 2020; García-Castellanos et al., 2020; Spatola et al., 2020), since it is physically unfeasible that Parathetyan water entering the eastern Mediterranean could have spread westward in a Mediterranean Basin isolated and desiccated during Stage 3 (Marzocchi et al., 2016; Stoica et al., 2016). By contrast, a Mediterranean almost completely full, dominated by non-marine waters from the major Mediterranean drainage systems (Roveri et al., 2008a) and from Eastern Paratethys (Flecker and Ellam, 2006; Vasiliev et al., 2010, 2017; Marzocchi et al., 2016; Van Baak et al., 2016; Grothe et al., 2020), has been proposed in the light of the occurrence of the same species of ostracods everywhere in the Mediterranean (Gliozzi et al., 2007; Stoica et al., 2016; Sciuto et al., 2018). The discovery of dwarf specimens of long-ranging planktic foraminifera species in the Lago-Mare of the Bajo Segura record (Corbí and Soria, 2016), the anomalous peak in the abundance of the calcareous nannofossil *Sphenolithus abies* underneath the M-P boundary in ODP site 968 (Castradori, 1998) and molecular biomarkers with hydrogen isotope compositions ($\delta D_{n-alkanes}$) similar to present-day marine settings (Vasiliev et al., 2017) point to some supply also from the Atlantic.

In a restricted Mediterranean Basin where several isotopically-distinct water sources are thought to have contributed to its hydrological configuration, $^{87}Sr/^{86}Sr$ ratios can be used to discriminate between the various sources of water (Flecker et al., 2002; Flecker and Ellam, 2006; Topper et al., 2011) and to infer phases of isolation or connectivity

(e.g., McCulloch and De Deckker, 1989). In most Mediterranean marginal basins (e.g., Apenninic sub-basins; Schildgen et al., 2014), however, the predominance of Mesozoic carbonates in the catchments ($^{87}Sr/^{86}Sr$ ratios vary from ~0.7071 to ~0.7076; McArthur et al., 2012) means that local run-off has a relatively low Sr isotope ratio, which could be similar to a mixture of the three potential sources of the Mediterranean Basin, i.e., Atlantic (~0.7090 during the late Messinian; McArthur et al., 2012), main Mediterranean rivers (e.g., Nile with 0.7060 and Rhône with 0.7087; Brass, 1976; Albarède and Michard, 1987) and Eastern Paratethys (0.7084–0.7085; Grothe et al., 2020), making local and Mediterranean inputs challenging to distinguish. By contrast, the adjoining Sorbas, Nijar and Vera basins in SE Spain all have present-day fluvial catchments dominated by Paleozoic mica schists and phyllites (Sanz de Galdeano and Santamaría-López, 2019) and Miocene volcanic rocks (e.g., Toscani et al., 1990; Zeck et al., 1998; Conticelli et al., 2009). Rivers draining these rocks have substantially higher $^{87}Sr/^{86}Sr$ ratios (>0.7100 on average; e.g., Zeck et al., 1998; Toscani et al., 1990; Conticelli et al., 2009). This contrast makes it possible to distinguish local fluvial supply to these Spanish marginal basins from the lower Sr isotope ratios of Mediterranean's water sources. We therefore investigated the hydrology of this cluster of marginal basins in SE Spain using new and published (McCulloch and De Deckker, 1989; Fortuin et al., 1995; Roveri et al., 2019) $^{87}Sr/^{86}Sr$ data measured on well-preserved ostracod valves of *Cyprideis* sp. from the latest Messinian deposits of the Sorbas (Zorreras Mb.), Nijar (Upper Mb. of Feos Fm.) and Vera (Unit 2) basins. The measured Sr isotope ratios correspond to the Sr isotopic composition of the water inhabited by the ostracods. The $^{87}Sr/^{86}Sr$ of each watersheds' lithology is used to estimate the local river water compositions, while a mass balance model is used to identify and quantify the different water sources feeding each marginal Spanish basins. Combining these geochemical data and model constraints with previous sedimentological and paleontological findings we provide insights into the Mediterranean's water level during the latest Messinian.

2. Geological setting

2.1. Evolution of the Neogene basins of the Betic Cordillera

The Sorbas-Nijar-Vera basins are NE-SW elongated depressions belonging to the Betic Cordillera in southern Spain (Fig. 1A; Sanz de Galdeano and Vera, 1991, 1992; Vera, 2000). The post-orogenic evolution of the arc-shaped Betic-Rif mountain belt is dominated by both vertical (Martinez-Diaz and Hernandez-Enrile, 2004; Capella et al., 2017) and strike-slip motions (Montenat and Ott d'Estevou, 1999; Jonk and Biermann, 2002) that generated narrow subsiding depressions filled with the erosional products of adjacent basement highs (Krijgsman et al., 2000; Vera, 2000, 2001; Braga et al., 2006; Capella et al., 2018). The subsiding basins of SE Spain were part of the Betic Corridor, a set of four narrow marine gateways that connected the Atlantic Ocean and the Mediterranean Sea via southern Spain during the late Miocene (Martín et al., 2014; Flecker et al., 2015; Krijgsman et al., 2018). From the latest Tortonian onwards, continuous uplift of the Betic-Rif system progressively changed the dimensions of the marine corridors in both Spain and Morocco (Krijgsman et al., 2006, 2018; Martín et al., 2014), inducing severe restriction of Mediterranean-Atlantic exchange, substantial hydrological reorganization of Mediterranean circulation patterns (Flecker et al., 2015 and references therein) and ultimately the MSC (Roveri et al., 2014a). While the Betic Corridor's internal basins (Lorca, Fortuna, Granada, Huércal-Overa, Campo Coy) were isolated before the Messinian, preserving evaporitic successions referred to as the "Tortonian Salinity Crisis of the eastern Betics" (Krijgsman et al., 2000; Corbí et al., 2012), the external basins (Malaga, Nijar, Sorbas, Vera, Murcia-Cartagena, Bajo Segura) contain sedimentary records of the Messinian Salinity Crisis (Fig. 1A; e.g., Fortuin et al., 1995; Fortuin and Krijgsman, 2003; Braga et al., 2006; Guerra-Merchán et al., 2010).
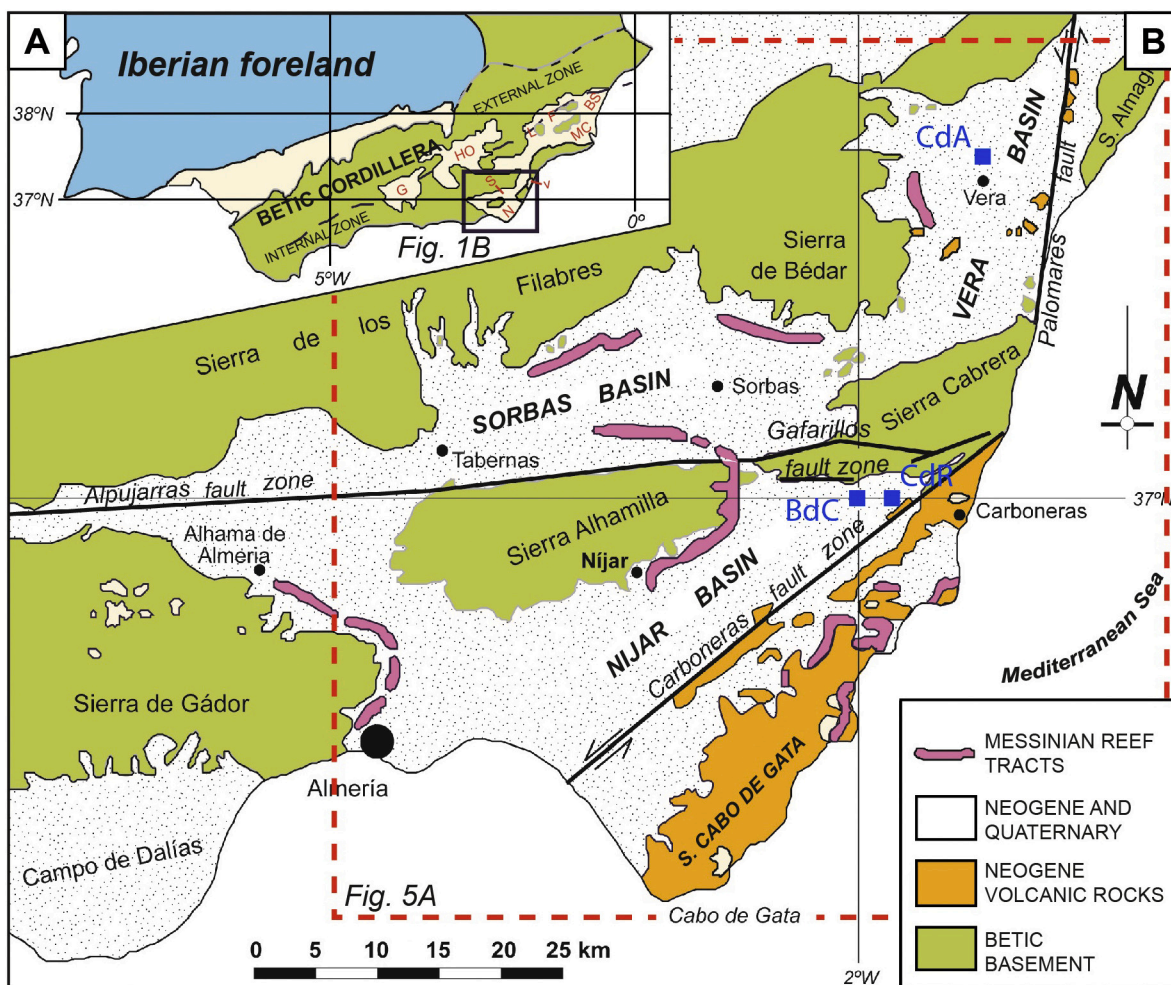
Fig. 1. A) Geological map of the Betic Cordillera showing the location of the internal (G=Granada, HO=Huércal-Overa, L=Lorca, F=Fortuna) and external (N=Nijar, S=Sorbas, V=Vera, MC=Murcia-Cartagena, BS=Bajo Segura) Neogene basins. B) Schematic geological map of the eastern end of the Betic Cordillera (modified after Fortuin and Dabrio, 2008). Blue squares indicate the location of the studied sections in the Nijar (BcD: Barranco de los Castellones; CdR: Cerro de los Ranchos) and Vera (CdA: Cuevas del Almanzora) sections. Samples' provenance from the Sorbas Basin is unknown. (For interpretation of the references to colour in this figure legend, the reader is referred to the web version of this article.)

2.2. Late Miocene connectivity evolution and stratigraphy of the Sorbas-Nijar basins

The Nijar and Sorbas basins are today separated from each other by the sierras de Gádor, Alhamilla and Cabrera (Fig. 1B). The Sierra de los Filabres and Sierra de Bédar border the Sorbas Basin to the north, while the Sierra de Gata (or Cabo de Gata, CdG) constitutes the SE edge of the Nijar Basin (Fig. 1B). Cabo de Gata is a volcanic complex belonging to the Alborán volcanic province, a 500–600 km long, SW-NE trending belt stretching from N Africa to SE Spain and characterized by magmatic activity of Neogene age (ca. 20 to 2 Ma; Zeck et al., 1998). During the Miocene, until the end of MSC Stage 1, both basins were connected to the Mediterranean, which made its entrance in the Nijar Basin from the south and in the Sorbas Basin through NW-SE trending corridors north to Nijar (Fortuin and Krijgsman, 2003; Fig. 1B). Despite the fact that sedimentation in both basins has been strongly affected by the activity of three major strike-slip fault zones, i.e., the NE-SW Serrata-Carboneras Fault, the E-W trending Gafarillos Fault Zone and the N-S Palomares Fault Zone (Montenat and Ott d'Estevou, 1999; Fig. 1B), the intimate communication between the Nijar and Sorbas basins is reflected in their similar pre-MSC Stage 2 successions.

The hundred meter thick pre-MSC infill of both basins unconformably overlies the metamorphic basement of the Betic Cordillera and, for the Nijar Basin only, the volcanic complex of Cabo de Gata (Fig. 1B). The

oldest sediments are of Serravallian-early Tortonian age (Brachert et al., 2002). The late Tortonian-early Messinian period is preserved in the marginal areas of the basins as fossil-rich calc-lithic arenites (Azagador Member of Turre Formation, Völk and Rondeel, 1964) and reef carbonates (Cantera Reef Member of Turre Formation; Völk and Rondeel, 1964). In the basin center, the deepest water facies are represented by epibathyal marls (Abad Member of Turre Formation; Fig. 2A). This unit is characterized by a well-developed, precession-controlled lithological cyclicity exemplified in the lower part by homogenous marls and more indurated, opal-CT-rich layers that change up-section to sapropelitic laminites, marls and chalks (van de Poel, 1991; Sierro et al., 2001 and references therein). Particular attention has been paid to the sediments of the MSC, because both Sorbas and Nijar preserve two of the most complete records of this period in the Mediterranean. The MSC starts here with the Yesares Formation (Dronkert, 1976; van de Poel, 1991; Krijgsman et al., 2001; Fortuin and Krijgsman, 2003; Lu, 2006), attributed to MSC Stage 1 (Fig. 2A). Locally in the Nijar Basin, vuggy limestones, limestone breccias, calciturbidites and sandstones belonging to the Manco Limestone Member pass upward, with an erosional contact, into dominantly detrital gypsum beds.

Sorbas-Nijar-Mediterranean connectivity was severed in the late Messinian by differential uplift of the basement highs, which resulted in the erosion of Paleozoic crystalline rocks (mostly mica schists and phyllites; Sanz de Galdeano and Santamaría-López, 2019), Permo-
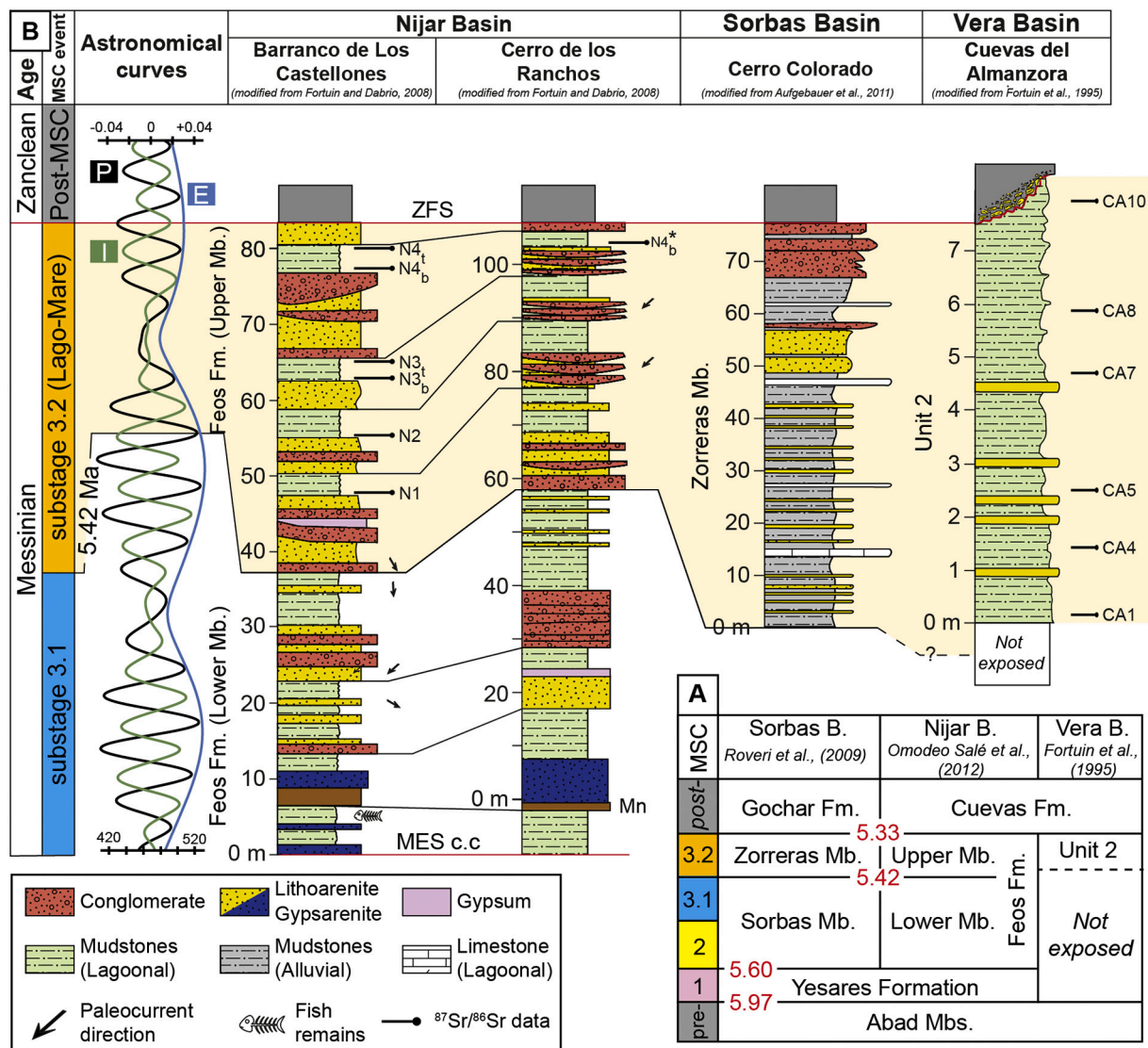
Fig. 2. A) More recent (and herein adopted) stratigraphic frameworks for the Sorbas, Nijar and Vera basins. Their correlation with the MSC consensus chronostratigraphic model of Roveri et al. (2014a) is also shown. Red numbers correspond to the age (in Ma) of each event. B) Stratigraphic log of the Barranco de Los Castellones and Cerro de los Ranchos in sections in Nijar and of the Cuevas del Almanzora section in Vera where some of the new and published 87Sr/86Sr ratios herein discussed come from. The Cerro Colorado section in Sorbas is only meant to show the stratigraphy and sedimentological features of the Zorreras Mb., since the exact provenance of the analyzed samples is unknown (see text). Correlations among the Nijar sections is based on Fortuin and Dabrio (2008). Astronomical tuning of the Nijar sections to climatic precession (P), 100 kyr eccentricity (E) and the 65°N insolation curve (I) of Laskar et al. (2004) is based on Hilgen et al. (2007). MES c.c.: Messinian Erosional Surface correlative conformity; ZFS: Zanclean Flooding Surface (see Subsection 3.1 for further insights). (For interpretation of the references to colour in this figure legend, the reader is referred to the web version of this article.)

Mesozoic sediments and early-middle Miocene volcanics of Cabo de Gata and their incorporation in Messinian strata (Roep et al., 1998; Fortuin and Krijgsman, 2003). The triple connection may have recurred during substage 3.1, when basinal marls and shallow-water carbonates with marine fauna (echinoids, scleractinians and bivalves) are found (Sorbas Mb. of Sorbas and Lower Mb. of the Feos Fm. in Nijar; Braga et al., 2006; Fig. 2A). The Nijar-Sorbas connection is believed to have been absent during substage 3.2, characterized in both the basins by fluvial sediments and fine-grained deposition in a subaqueous environment interpreted as an endorheic lake (Zorreras Mb. of Sorbas and Upper Mb. of the Feos Fm. in Nijar; Fortuin and Krijgsman, 2003; Braga et al., 2006; Aufgebauer and McCann, 2010; Fig. 2A). Only for the Nijar Basin, an intermittent connection with the Mediterranean persisting throughout Stage 3 has been proposed on the basis of the observed ostracod assemblages of the Feos Fm. (Stoica et al., 2016). The Sorbas-Nijar-Mediterranean connection was undoubtedly restored at the base

of the Zanclean with the deposition of foraminifer-rich biocalcarenites (Gochar Fm. in Sorbas and Cuevas Fm. in Nijar; Aguirre, 1998; Roep et al., 1998; Roveri et al., 2019; Fig. 2A).

2.3. Late Miocene connectivity evolution and stratigraphy of the Vera Basin

The Vera Basin is located to the NE of the Sorbas and Nijar basins, enclosed by the Sierra de Bédar to the NNW, Sierra Cabrera to the S and Sierra Almagrera to the NE (Fig. 1B). The late Tortonian-Messinian (i.e., pre-MSC) sedimentation in Vera was similar to the adjacent Sorbas and Nijar basins, with pelagic marls passing upslope into reef carbonates (Fig. 2A; Fortuin et al., 1995). In Vera, turbidites, slumps and volcanites are frequently found in the "Abad" marls (Unit 1 or Santiago Beds; Fortuin et al., 1995) and related to the initiation of the activity of the Palomares fault (Fortuin et al., 1995). Late Messinian primary

evaporites are absent in Vera. Instead, the Santiago beds are unconformably overlain by shallow-water laminated mudstones containing Black Sea-type brackish-water ostracods (Unit 2; Fortuin et al., 1995; Stoica et al., 2016; Caruso et al., 2019), which in turn are covered by marine marls of Pliocene age (Cuevas Fm. or Unit 3; Fortuin et al., 1995). Reworked gypsum occurs associated with olistostrome-like deposits in the area surrounding the village of Garrucha, suggesting that evaporites probably were deposited in Vera as well, but subsequently removed by sin- to post-depositional erosion (Fortuin et al., 1995).

In terms of connectivity, the stratigraphy of the Vera Basin indicates that it was part of the Sorbas-Nijar-Mediterranean system until the onset of the MSC and possibly during evaporite deposition (Fortuin et al., 1995; Fortuin and Krijgsman, 2003). Splitting of the Sorbas-Nijar-Vera system is thought to have occurred in late Yesares times probably due to the uplift of the Sierra Cabrera (Fortuin et al., 1995) and persisted throughout the Lago-Mare stage, when an endorheic lake was filling the Vera Basin (Benson and Rakic-El Bied, 1991; Caruso et al., 2019). An opposite interpretation described a continuous Mediterranean connection during the Lago-Mare phase, with Vera depicted as an embayment of the Mediterranean, which was therefore topped up with water (Stoica et al., 2016).

3. The post-evaporitic records

3.1. Feos Formation (Nijar)

Following the lithostratigraphic scheme of Omodeo Salé et al. (2012), the Feos Formation has been subdivided into two members sandwiched between two major stratigraphic surfaces: (I) the Messinian erosional surface (MES) and its correlative conformity (MES c.c.) at the base; (II) the Zanclean flooding surface (ZFS) at the top (Fig. 2B). The Lower Member is mainly a resedimented and gypsum-bearing chaotic unit overlain by alternating silt and reworked gypsum crystals with mudstones. Noticeable here is the presence of a brown-black Mn-hydroxide-enriched level ~ 10 m above the boundary with the Yesares Formation (Fig. 2B). This bed is a useful marker that can be traced throughout the southeastern sector of the basin (Fortuin and Krijgsman, 2003). Approximately 20 m above this marker bed, the boundary with the more terrigenous and less carbonate-rich Upper Member is placed, denoting an important change in depositional environment (Fortuin and Krijgsman, 2003; Omodeo Salé et al., 2012).

The Upper Member is characterized by red to grey coarse-grained continental intervals (conglomerates and sandstones) alternating with white to grey, laminated chalky-marl (Figs. 2B, 3A; Fortuin and Krijgsman, 2003; Omodeo Salé et al., 2012). Four complete alternations and
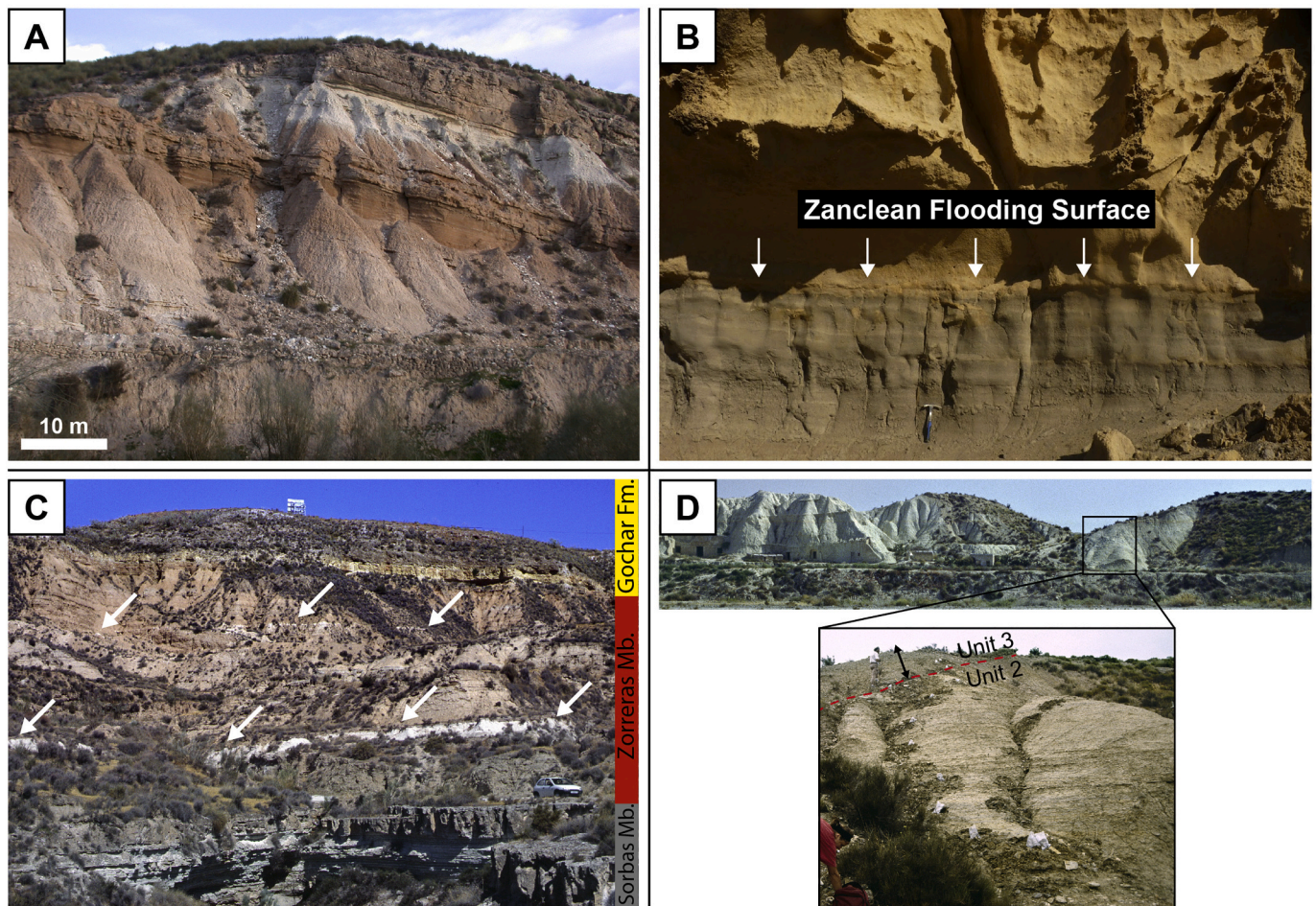
Fig. 3. A) Part of the type section of the Feos Fm. along the river Alias at Los Feos. The cliff section (herein named El Salto del Lobo) shows the superposition of a thick pink and reddish continental interval, followed by white ostracods-bearing laminated mudstones, passing upwards into a next coarse clastic, continental interval. B) Photograph of the conformable stratigraphic contact between the uppermost Lago-Mare sandstone of the Feos Fm. and the Zanclean biocalcarenites of the Cuevas Fm. in the Barranco de los Castellones section (rock hammer for scale). C) Photograph showing the largely red continental sediments of the Zorreras member locally interrupted by white limestones (white arrows). The gradual transition of the Zorreras Mb. from the Sorbas Mb. underneath and to the Gochar Fm. on top is also appreciable. Car for scale. D) Panoramic view of the Cuevas del Almanzora section and detail of the sampling site logged in Fig. 2B. (For interpretation of the references to colour in this figure legend, the reader is referred to the web version of this article.)

one incomplete cycle are observed, sealed by the marine Pliocene strata of the overlying Cuevas Formation (Figs. 2B, 3B). The sharp lithological transition to open marine deposits is slightly erosional at the basin margins but appears to be conformable above a fluvial sandstone in the central parts of the basin (Fig. 3B; Fortuin and Krijgsman, 2003).

Based on the assumption that these alternations are precessional cycles, the Lower Mb.-Upper Mb. transition has been cyclostrati-graphically dated at 5.42 Ma in its better exposed section of Barranco de los Castellones (37°00′51.1″N; 2°00′05.7″W; Omodeo Salé et al., 2012; Fig. 2B). This age corresponds to the substage 3.1–3.2 transition of the consensus model (Roveri et al., 2014a) as defined in the Northern Apennines (Roveri et al., 2008a and references therein).

The four fine-grained intervals of Nijar's Upper Member host a microfaunal assemblage mainly composed of oligohaline, Black Sea-type ostracods mixed with marine foraminifera (Fortuin and Krijgsman, 2003; Bassetti et al., 2006). Bassetti et al. (2006) recognized significant variations in ostracod species within each pelitic bed. They differentiated two main assemblages: the first occurs at the base of the fine-grained hemicycle and is characterized by low species diversity dominated by *Cyprideis agrigentina* with rare specimens of *Tyrrhenocythere* sp. The second assemblage, which occurs at the top of each pelitic bed, has a higher species diversity with abundant Parathethyan-like specimens belonging to different genera (e.g., *Cyprideis*, *Candona*, *Loxornicula*, *Amnicythere*, *Loxoconcha*). It is noteworthy to point out that Bassetti et al. (2006) claimed that these ostracod species have no affinity with the coeval Parathethyan species. However, Stoica et al. (2016) showed that this conclusion arose from the employment of different taxonomic concept. Consequently, Parathethyan ostracods also inhabited the Nijar Basin.

The foraminiferal assemblage found in the pelitic intervals is considered to be in situ by Aguirre and Sánchez-Almazo (2004), but physically reworked by all others (Fortuin and Krijgsman, 2003; Bassetti et al., 2006; Fortuin and Dabrio, 2008; Omodeo Salé et al., 2012).

3.2. Sorbas-Zorreras members (Sorbas Basin)

The package of sediments sandwiched between the Yesares Gypsum and the Pliocene in Sorbas are subdivided into two members: the Sorbas Member and the Zorreras Member.

The Sorbas Member, studied in detail by Roep et al. (1998), is ~70 m thick and it consists of marls, silts and sands arranged in three para-sequences recording base-level fluctuations that pass marginally into the so-called Terminal Carbonate Complex (TCC), a carbonate platform system constituted by heterogeneous limestones and minor coarse sili-ciclastic sediments (see Roveri et al., 2009 and Bourillot et al., 2010 for insights and references). As such, overall the Sorbas Member is interpreted as having been deposited in a shallowing-upward environment surrounded by shallower carbonate factories and emerged areas supplying the coarser siliciclastic fraction (Roep et al., 1998; Braga et al., 2006; Aufgebauer and McCann, 2010).

The Sorbas Member and TCC are conformably overlain by the up to 75 m thick Zorreras Member (Fig. 3C). This unit mainly consists of azoic paleosoils, reddish silt- and sandstones, grey-coloured sandstones and conglomerates with some intercalated carbonate beds (Fig. 3C), whose exact number is debated from two to four (Roveri et al., 2009, 2019; Aufgebauer and McCann, 2010). These limestones range in thickness from 95 cm to 120–152 cm. They are whitish, massive, with little evidence of internal structure and only contain rare ostracod specimens mostly belonging to the euryhaline *Cyprideis* sp., *Loxocorniculina dja-farovi* and freshwater species of the family *Limnocytheridae* (Roep and Van Harten, 1979; Aufgebauer and McCann, 2010). In some outcrops, a thin bed (3–10 cm) of green-grey-coloured mudstone is present below the upper carbonate bed and this contains thick laminae (0.6–1 cm) of bituminous material (Aufgebauer and McCann, 2010). At present, the Zorreras Member is interpreted as representative of the repetitive development of alluvial fan systems sporadically interrupted by the

expansion of lacustrine conditions related to either intra-basinal flood-ing events (Aufgebauer and McCann, 2010) or water incursions from the Nijar Basin (Mather and Stokes, 2001; Fortuin and Krijgsman, 2003). Whatever the provenance of the water was, the position of the carbonate layers indicates that subaqueous conditions established suddenly and lasted ephemerally (Aufgebauer and McCann, 2010).

Over the years, the attribution of the Sorbas and Zorreras members to the MSC stages, likewise the age boundaries, changed and is still controversial (see summary in Krijgsman et al., 2001 and Roveri et al., 2019). In this paper we adopt the more recent chronostratigraphic framework of Roveri et al. (2009, 2019), which attributed the Sorbas member to Stage 2 and substage 3.1 and the Zorreras member to the Lago-Mare phase (Fig. 2A).

3.3. Unit 2 (Vera Basin)

Unlike in Nijar and Sorbas, the Lago-Mare phase in Vera is only expressed by ~12 m of varicoloured laminated mudstones (Unit 2 of Fortuin et al., 1995; Figs. 2A-B), whose best exposure is found in the Cuevas del Almanzora section (37°17′00″N; 1°50′33″W) (Fig. 3D; Montenat and Bizon, 1976; Benson and Rakic-El Bied, 1991; Fortuin et al., 1995; Stoica et al., 2016; Caruso et al., 2019). An ostracod fauna with Parathethyan affinity typifies the mudstones (Stoica et al., 2016; Caruso et al., 2019). The ostracod fauna changes in diversity from the base of the section, where it is dominated by *Cyprideis* sp., to the top, which is rich in species typical of the Pontian of the Euxinic and Caspian basins (Stoica et al., 2016), similarly to the mudstone horizons of the Upper Mb. of the Feos Fm. in Nijar. The lower contact of these sediments with older lithologies is not exposed, while on top they are capped by an erosional surface draped by conglomeratic accumulations (Fortuin et al., 1995; Stoica et al., 2016; Caruso et al., 2019).

4. Material and methods

4.1. Evaluation of ostracods $^{87}Sr/^{86}Sr$ isotope ratios

4.1.1. Samples selection

Strontium ($^{87}Sr/^{86}Sr$) isotope compositions were obtained from the calcitic valves of the ostracod *Cyprideis* sp. picked from the uppermost four pelitic strata of the Upper Member of the Feos Formation in the Barranco de los Castellones section in Nijar (Fig. 2A), the lowermost limestone horizon of Sorbas (unknown locality) and the marly mud-stones of Vera in an outcrop next to the Cuevas del Almanzora section. In the Nijar Basin, two additional samples, one from the Cerro de los Ranchos section (Fig. 2B) and one from an outcrop (named El Salto del Lobo; Fig. 3A) along the river Alias, were studied. In the stratigraphic interval expressing the Lago-Mare stage in these three basins the os-tracods are an archive of the water Sr chemistry, because during valves secretion they extract Sr from the water in which they dwelt (Figs. 6A-B) with isotopic fractionation effects that may occur during the liquid-solid transition but that are removed during data reduction (Hajj et al., 2017 and references therein). All the other lithologies present in the strati-graphic intervals studied (conglomerates, sands and reddish pelites; Fig. 2B) were deposited in a continental environment and lack abiotic and/or biotic phases suitable for Sr analyses.

In the Barranco de los Castellones section (Nijar Basin), only six samples of the pelitic intervals of the Feos Fm. contained sufficient (e.g., 4) well-preserved ostracod valves to permit Sr isotope analysis to be carried out. In cycle I and II, both the measurements come from the bottom of the pelitic layer immediately above the transition from the underlying continental conglomerates, while in cycles III and IV two samples were obtained from the bottom and the top of the pelitic layers (Fig. 2B). The new data from Sorbas, Nijar and Vera are intended to update and widen the dataset already built in the past by McCulloch and De Deckker (1989) for the Sorbas Basin, Roveri et al. (2019) for the Nijar Basin and Fortuin et al. (1995) for the Vera Basin. Roveri et al. (2019)

measured one sample from the uppermost mudstone horizon of the Feos Upper Mb. in the Barranco de los Castellones section. Fortuin et al. (1995) run seven measurements of samples from the Cuevas del Almanzora section. Of these data point, one has not been considered due to a large analytical error. McCulloch and De Deckker (1989) did not specify from which of the two (or four) lacustrine levels their Sorbas measurements came from (Fig. 2B). New and published measurements have been carried out on valves of *Cyprideis* sp. We have chosen to be consistent with the species analyzed to minimize the possible effects of biological fractionation (i.e., the vital effect), although Sr appears only to undergo significant fractionation in its $\delta^{88}Sr/^{86}Sr$, while for the radiogenic $^{87}Sr/^{86}Sr$ used here fractionation is normalized out during the measurement (e.g., Hajj et al., 2017).

4.1.2. Samples preparation and measurement

Single valves (~10) of the selected specimens for each sample were first repeatedly cleaned in Milli-Q water by mild ultrasonification lasting 30 s, after which the liquid and any contamination was pipetted off. Visual inspection using binocular microscope and SEM indicates that all adherent clays had been removed by this process. The valves were then placed in acid-cleaned 1 ml centrifuge tubes and dissolved in ~0.5 ml 5 N acetic acid for ~2.5 h. After centrifuging at 12,000 rpm for 8 min, 400 µl of the fluid was taken out and dried overnight in open, acid-cleaned, savillex PFA 24 mm rocket beakers at ~110 °C. Two drops of concentrated HNO_3 were added to all dried samples, which were then taken up in 3 N HNO_3. The elemental composition (Ca, Sr, Mg and Mn) was determined on a weighted aliquot of this solution using a Liberty II Varian ICP-AES, in order to assess the total amount of strontium. Subsequently, based on the ICP-AES analyses ~1 microgram of strontium was purified using column separation with ion-specific Sr-spec resin.

The $^{87}Sr/^{86}Sr$ ratio was analyzed by thermal ionisation mass spectrometry using a Finnigan MAT 262, mostly following the method as described in Beets (1991) and Fortuin et al. (1995). Briefly, aliquots of ~500 ng of the selected samples were loaded on single, zone-refined rhenium filaments with a mixture of $TaCl_5$ and H_3PO_4 emitter-fluid. During the measurements of the Lago-Mare ostracods, three NBS 987 standards were added to the sample turret to monitor the reproducibility of the measurements. Also a procedural blank, including separation chemistry and loading, was measured. Average NBS 987 $^{87}Sr/^{86}Sr$ is 0.710247 ± 0.000011 (1sd; $n = 3$), whereas the in-run precision of individual measurements was better than 0.000010 (1sd). The blank was determined at 0.124 ng Sr, which is less than 0.025% of the average amount of loaded Sr and therefore negligible. All isotope analyses were carried out in a clean-lab environment at the Vrije Universiteit Amsterdam.

4.2. Mass-balance calculations

The $^{87}Sr/^{86}Sr$ isotopic composition of Sr dissolved in a subaqueous sedimentary environment is dependent upon the $^{87}Sr/^{86}Sr$ isotopic composition and Sr concentration of all the reservoirs that contribute to shape the water body (e.g., Doebbert et al., 2014; Zielinski et al., 2017). Knowing the strontium parameters (i.e., $^{87}Sr/^{86}Sr$ ratios and strontium concentration) and the relative contribution of each water source, the $^{87}Sr/^{86}Sr$ isotopic composition ($Sr^{87/86}_{Mixture}$) of a mixture of multiple (1, 2, … n) water sources can be calculated by means of a chemical mass balance approach (e.g., Placzek et al., 2011; Doebbert et al., 2014; Grothe et al., 2020):

$$Sr^{87/86}_{Mixture} = F_{R1} \cdot {}^{87}Sr/{}^{86}Sr_{R1} + F_{R2} \cdot {}^{87}Sr/{}^{86}Sr_{R2} + \ldots + F_{Rn} \cdot {}^{87}Sr/{}^{86}Sr_{Rn} \quad (1)$$

where $F_{R1, 2, \ldots}$ is the fraction of Sr that each source contributes and $^{87}Sr/^{86}Sr_{R1, 2, \ldots}$ is the Sr isotope ratio (dimensionless) specific to each reservoir. In turn, the Sr fractional contribution (F) of individual sources is:

$$F_{R1} = \frac{[Sr]_{R1} \cdot d_1}{[Sr]_{R1} \cdot d_1 + [Sr]_{R2} \cdot d_2 + \ldots + [Sr]_{Rn} \cdot d_n} \quad (2)$$

where $[Sr]_{Rn}$ (mg/l) is the strontium concentration and d_n (dimensionless) is the fraction of discharge of each water source.

Using these equations, we developed a strontium mass-balance model to help constrain the evolution of the Sr isotopic composition of the Sorbas, Nijar and Vera water bodies inhabited by the ostracods, varying the mixing proportion between the different water sources. We explored the mutually exclusive possibilities of a system of isolated endorheic lakes supplied only by intrabasinal inputs (surface runoff and groundwater; Fig. 6A) and of a system of basins that received additional extrabasinal water (and therefore Sr) from the Mediterranean Basin (Fig. 6B).

The model requires knowledge of the Sr flux into the basins from every major source (Table 1). As for the runoff terms, given the lack of direct measurements on present-day analogs we considered each of the main catchment-forming lithologies (Fig. 5; see Subsection 5.2) to have been a source of Sr with the same $^{87}Sr/^{86}Sr$ ratio as the one measured on the bulk rock, while the values of strontium concentration for source (herein mentioned as local rivers) are based on [Sr] observed in modern rivers draining carbonate and silicate rocks (e.g., Brenot, 2006; Doebbert et al., 2014; Zielinski et al., 2017). The Sr concentration of the carbonate end member has been adjusted to a higher value than the average (e.g., Brenot, 2006) to account for the higher solubility relative to igneous or metamorphic basement rocks. The assumption of using $^{87}Sr/^{86}Sr$ ratios of bedrocks as analogue of the $^{87}Sr/^{86}Sr$ ratios of rivers derives from the fact that Sr^{2+} dissolved in rivers inherits the isotope signature of the rocks weathered in the catchment (Brenot, 2006; Doebbert et al., 2014; Hajj et al., 2017; Zielinski et al., 2017). $^{87}Sr/^{86}Sr$ value of 0.7086 for the Mediterranean water is (roughly) the midpoint value of the range of Sr values (0.7085–0.7087; Fig. 4A) measured on ostracods recovered from the intermediate basin of Caltanissetta in Sicily (Grossi et al., 2015) and from DSDP sites drilled in the central Mediterranean basins (McCulloch and De Deckker, 1989). Three values of Sr concentration have been employed: an extremely high value of 8 mg/l, which corresponds to the value of the present-day seawater (Veizer, 1989), an extremely low value of 0.5 mg/l, which is a more fluvial-like value, and an intermediate (and more likely) value of 1 mg/l (see Subsection 6.4 for more insights). The input of Sr from groundwater is the major unknown as it cannot be realistically reconstructed and sampled and present-day estimates are absent. For this reason, the groundwater component is not incorporated in the model.

Mass balance calculations can be applied to n-component systems

Table 1
Summary of the $^{87}Sr/^{86}Sr$ and Sr concentration of each water source considered in the mass-balance calculation. $^{87}Sr/^{86}Sr$ isotope ratio of river 5 and 6 are the arithmetic average of the mixed sources.

| Water source	$^{87}Sr/^{86}Sr$ (range)	Strontium concentration [Sr] (mg/l)	References
Late Messinian Mediterranean water	0.7086	8, 1 and 0.5	Text, Section 4.2
River 1 (Sch)	0.726545	0.035	Text, Sections 4.2 and 5.2
River 2 (Dol)	0.708612	0.260	Text, Sections 4.2 and 5.2
River 3 (Orth)	0.713684	0.035	Text, Sections 4.2 and 5.2
River 4 (Vol)	0.712496	0.035	Text, Sections 4.2 and 5.2
River 5 (Sch + Orth)	0.720115	0.035	Text, Sections 4.2 and 5.2
River 6 (Sch + Orth +Vol)	0.712668	0.035	Text, Sections 4.2 and 5.2
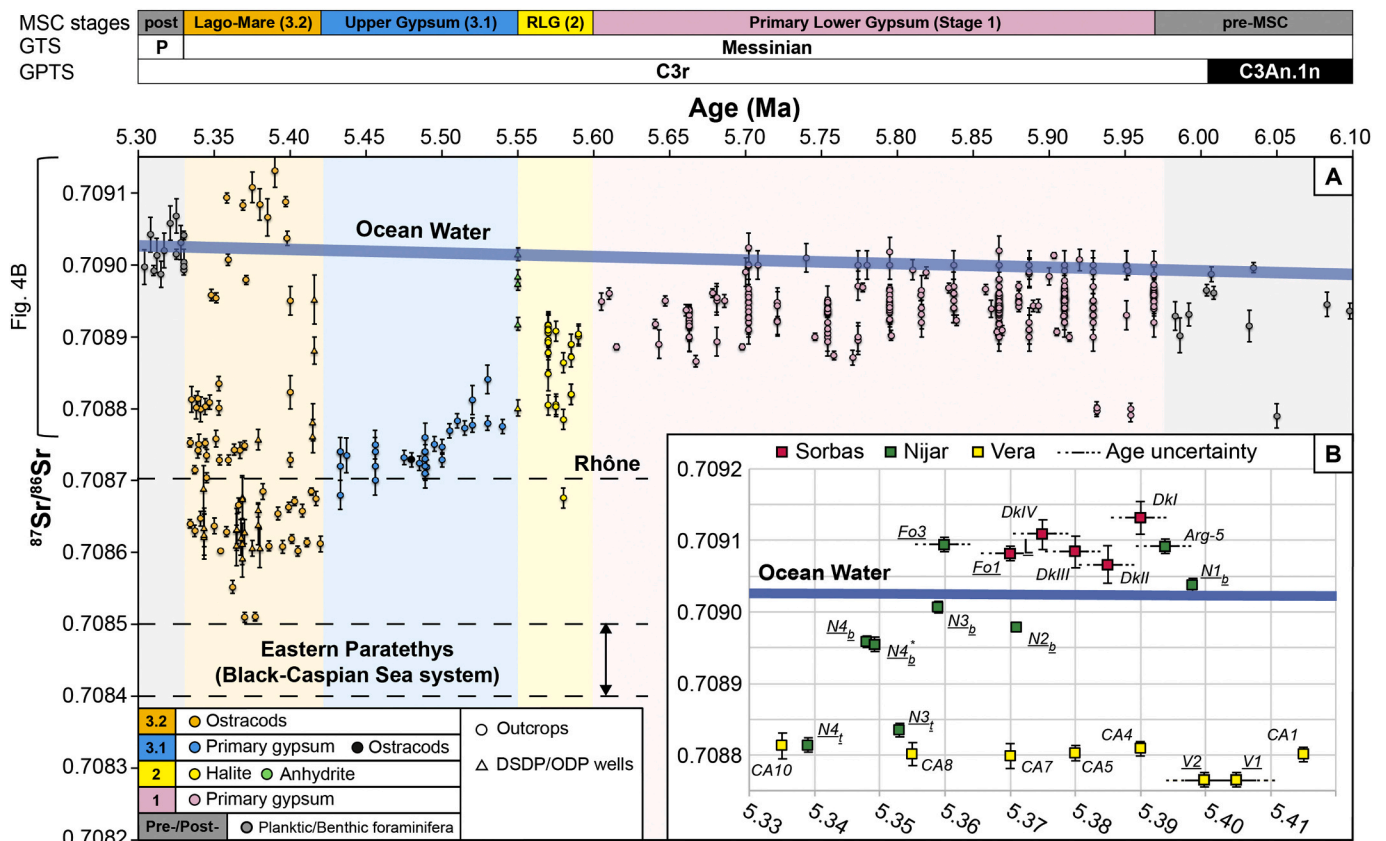
Fig. 4. A) Compilation of $^{87}Sr/^{86}Sr$ isotope data for the Mediterranean during the Messinian Salinity Crisis. A cyclostratigraphic age has been assigned to each sample according to the chronostratigraphic framework of Roveri et al. (2014a) for outcropping sections and Roveri et al. (2014b) for DSDP and ODP cores. Error bars indicate analytical error which is so small in some cases that no error bars are visible at this scale. Mediterranean $^{87}Sr/^{86}Sr$ data are derived from: McKenzie et al. (1988); McCulloch and De Deckker (1989); Müller and Mueller (1991); Fortuin et al. (1995); Flecker and Ellam (1999, 2006); Keogh and Butler (1999); Lugli et al. (2007, 2010); Roveri et al. (2014b, 2019); Schildgen et al. (2014); Evans et al. (2015); Grossi et al. (2015); Karakitsios et al. (2017); Reghizzi et al. (2017, 2018); García-Veigas et al. (2018). This data set has been compiled and evaluated and is available in the supplementary information (Supplementary material S1). Ocean water ratios are from McArthur et al. (2012); Black-Caspian Sea data are from Grothe et al. (2020); Rhône value is from Albarède and Michard (1987). B) Detailed $^{87}Sr/^{86}Sr$ record for Lago-Mare data from the Sorbas, Nijar and Vera basins and the coeval ocean ratio. Vera's values from the Cuevas del Almanzora section (Fortuin et al., 1995) are plotted using the chronostratigraphic framework of Stoica et al. (2016) and Caruso et al. (2019). New Nijar values generated during this project from the Barranco de Los Castellones and Cerro de los Ranchos sections are plotted using the chronostratigraphic framework of Hilgen et al. (2007). For the remaining values, age uncertainties are present. Underlined sample labels refer to the new measurements generated in this work. See supplementary material S2 for references of each datum.

(Eq. (1)), but the results are difficult to represent graphically. Accordingly, here we apply the procedure considering each basin as a three-component system (only local rivers in the lacustrine scenario; local rivers and Mediterranean water in the lagoonal scenario; Fig. 6) and we plot the isotopic signature of each mixture on a ternary diagram (Fig. 7). When the Mediterranean is not part of the system (i.e., lacustrine scenario; Fig. 6A), three continental fluvial sources are considered in the model (Figs. 7A-B). When the Mediterranean is considered (i.e., lagoonal scenario; Fig. 6B), only two riverine sources are taken into account (Figs. 7C-E) by combining those with the same Sr concentration (see Table 1) and calculating the arithmetic mean of the $^{87}Sr/^{86}Sr$ ratios of the individual sources. A detailed explanation of the approach pursued to constrain model results is provided in Subsection 5.3.

5. Results

5.1. $^{87}Sr/^{86}Sr$ isotope ratios of Spanish (Lago-Mare) ostracods

The new $^{87}Sr/^{86}Sr$ values from the Sorbas, Nijar and Vera basins are comparable with the values obtained by McCulloch and De Deckker (1989), Fortuin et al. (1995) and Roveri et al. (2019) from the same source material (Fig. 4B, Supplementary material S2).

Overall, the $^{87}Sr/^{86}Sr$ isotope ratios from these three Spanish basins encompass a wide range of values (from 0.708764 to 0.709131) straddling the ocean water ratio during the Lago-Mare phase (~0.7090; McArthur et al., 2012; Fig. 4B). Other than one sample (N1b) from Nijar Basin's Sr isotope record (0.708814–0.709099) none of the data are within error of coeval ocean water (0.709022–0.709026; McArthur et al., 2012; Fig. 4B), but the Nijar record links the higher values recorded in Sorbas (0.709066–0.709131; Fig. 4B), with much lower ones from Vera that are close to published ratios (<0.7088) typical of Lago-Mare sediments (substage 3.2) elsewhere in the Mediterranean (Fig. 4A).

Despite the low resolution of the data, the $^{87}Sr/^{86}Sr$ isotope record of the astronomically tuned Barranco de los Castellones section in Nijar (Fig. 2B) provides us with some hints as to the variation in isotopic composition of the water mass at subprecessional scale. The measured $^{87}Sr/^{86}Sr$ for cycle I plots within error of coeval global seawater Sr isotope ratios, while the other values from the base of the pelitic beds are all less radiogenic than ocean water (Fig. 4B). The samples from the upper parts of cycles III and IV are substantially lower than the rest of the Nijar data (0.708835–0.708814, respectively) and they are similar to values measured from substage 3.2 ostracods that inhabited the neighbouring Vera Basin (Fig. 4B).

5.2. Bedrock $^{87}Sr/^{86}Sr$ isotope ratios

Measurements of present-day $^{87}Sr/^{86}Sr$ ratios are available for all the main lithologies forming the crystalline basement and the overlying sedimentary covers in the watershed of the three marginal Spanish basins (Fig. 5A; see Supplementary material S2). We group these rock-types into four categories: para-derived rocks (i.e., phyllites and mica schists), ortho-derived rocks, volcanic rocks and dolostones (Fig. 5B).

The sierras de los Filabres and de Bédar to the north of the Sorbas and Vera basins consist of tectonic units belonging to the Nevado-Filabride complex (Sanz de Galdeano and Santamaría-López, 2019). Here, both para- and ortho-derived metamorphic rocks are found (Fig. 5A). The recent cartography of the western side of the Sierra de los Filabres by Sanz de Galdeano and Santamaría-López (2019) revealed that para-derived rocks are by far the more widespread. Among them, high-grade Paleozoic (±Mesozoic) phyllites and mica schists are the major constituent, with subordinate quartzites and sandstones (Fig. 5A; Sanz de Galdeano and Santamaría-López, 2019). These meta-sediments have highly radiogenic $^{87}Sr/^{86}Sr$ isotope ratios (0.713310–0.731679; Arribas Jr. et al., 1995; Nieto et al., 2000; Kirchner et al., 2016; Fig. 5B), compatible with $^{87}Sr/^{86}Sr$ values carried by the same rocks of the same age forming the metamorphic basement of the Mesozoic covers in Tuscany, Italy (0.713310–0.724882-0.738229; Conticelli et al., 2009). Ortho-derived rocks (e.g., metabasites, ophiolites, gneiss) of ages ranging from the Carboniferous to the Paleocene are found as isolated intrusions. These rocks are characterized by highly variable $^{87}Sr/^{86}Sr$ values (Puga et al., 2002), ranging from very low (0.703243) to very high (0.729459) ratios. Rare occurrence of Triassic marbles are also observed (Sanz de Galdeano and Santamaría-López, 2019), but no measurements of their Sr ratios are available.

In general, the abundance of carbonates, especially Triassic (possibly also Jurassic) dolomites, is relatively higher in the Sierra Alhamilla and Sierra Cabrera bordering the Nijar and Vera basins than in the sierras de los Filabres and de Bédar (Fig. 5A). The $^{87}Sr/^{86}Sr$ values of these carbonate bedrock lithologies range between a minimum of 0.707606 to a maximum of 0.710737 (Arribas Jr. et al., 1995; Conticelli et al., 2009; Mueller et al., 2020), averaging 0.708612 (Fig. 5B). These values are higher than the range predicted for the catchment limestones of both Triassic (from 0.707663 at 251.9 Ma to 0.707335 at 201.3 Ma, average of 0.707761; McArthur et al., 2012) and Jurassic age (from 0. 707335

at 201.3 Ma to 0.707189 at 145 Ma, average of 0.707182; McArthur et al., 2012). This aspect is common in metamorphic settings where carbonates are surrounded by silicate-rich rocks with high $^{87}Sr/^{86}Sr$ and is generally related to post-depositional processes that cause phyllosilicate mineral phases with radiogenic $^{87}Sr/^{86}Sr$ ratios to disseminate in limestones, making Sr isotope composition of these carbonates more radiogenic (e.g., Bickle et al., 2001).

An important source of allochthonous material supplied to the Nijar Basin is derived from the Sierra de Gata to the SE (Figs. 1B, 5A). The Cabo de Gata volcanic complex is mainly made up of Burdigalian-Pliocene volcanic rocks and minor leucogranitic intrusions intercalated within the Miocene and older sedimentary fill and resting discordantly over the basement rocks (Zeck et al., 1998). The younger (i.e., Messinian-Pliocene) lithologies are ultrapotassic rocks (lamproites: fortunites, jumillites, verites) and alkali-basalts that form only small and widely scattered bodies at the two southern and northern extremes of the Sierra de Gata (Zeck et al., 1998). The core of the complex is concentrated in its central parts and is made up of calc-alkaline volcanics (e.g., andesite; Zeck et al., 1998). Several (i.e., > 80 to our knowledge) $^{87}Sr/^{86}Sr$ isotope ratios of the calc-alkaline rocks are available from localities spanning the entire extent of the Sierra (Toscani et al., 1990; Arribas Jr. et al., 1995; Zeck et al., 1998; Conticelli et al., 2009). Cabo de Gata volcanics are grouped in a relatively well-defined cluster of very radiogenic isotopic values between 0.709691 and 0.716403 (Toscani et al., 1990; Arribas Jr. et al., 1995; Zeck et al., 1998; Conticelli et al., 2009; Fig. 5B).

Neogene magmatic rocks of the Alborán volcanic province also occur in the Vera Basin (Figs. 1B, 5A). These rocks are dated to the early Messinian (see Conticelli et al., 2009 for references) and are also characterized by high $^{87}Sr/^{86}Sr$ isotope ratios, ranging from 0.721029 to 0.722831 (Conticelli et al., 2009).

5.3. Model results

Mass balance modelling of the Sr isotope signal of the Spanish marginal basins produces a wide range of $^{87}Sr/^{86}Sr$ ratios (Fig. 7). Ideally, the Sr fluxes for each of the water sources would constrain the mixing proportion required to reproduce each measured Messinian $^{87}Sr/^{86}Sr$ ratio. Unfortunately, reliable values for Messinian fluvial Sr fluxes cannot be obtained directly, but instead are deduced from the
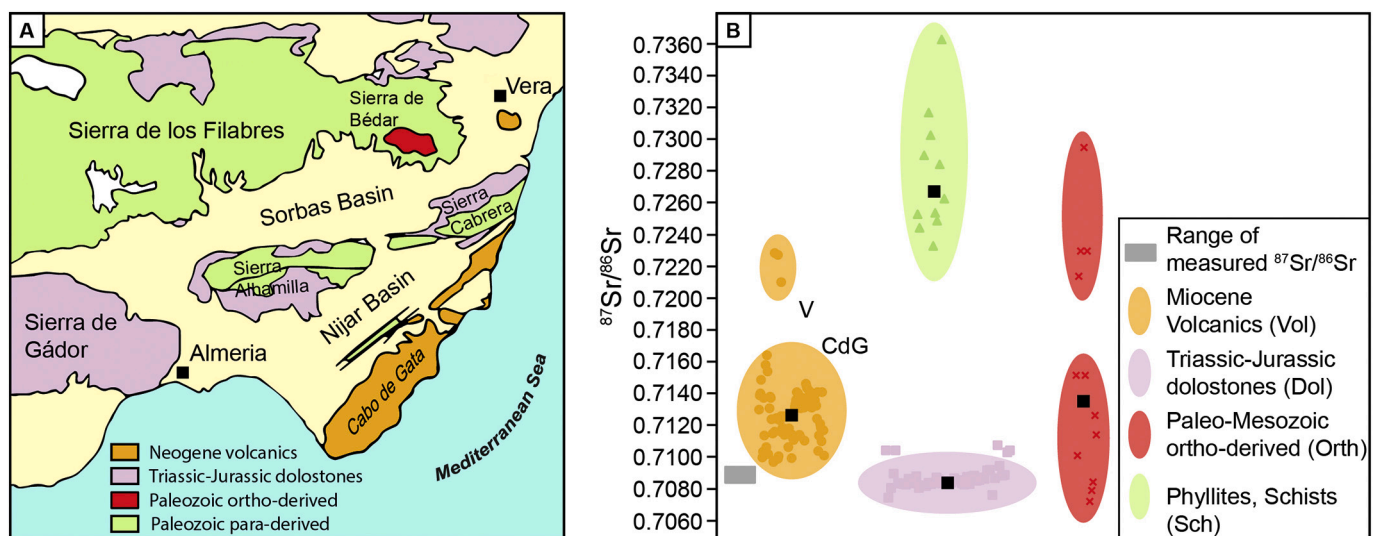
Fig. 5. A) Simplified geological map of the sierras surrounding the Sorbas, Nijar and Vera basins (modified from Murillo-Barroso et al., 2019 and Sanz de Galdeano and Santamaría-López, 2019). B) Delimitation of isotopic fields of the main catchments-forming lithologies in the $^{87}Sr/^{86}Sr$ isotopic ratios. Analytical errors are smaller than the symbols. Black squares indicate the average $^{87}Sr/^{86}Sr$ isotopic ratio of each isotopic field, which has been employed in the mass-balance calculation (values are listed in Table 1).

catchment's geology (Fig. 5B). To do this, we use the standard assumption that catchment area is proportional to discharge (e.g., Placzek et al., 2011). This means that the larger the volume of a specific lithology in the catchment, the more influence it has over the Sr flux of the river draining the catchment. The mountains surrounding the Sorbas, Nijar and Vera basins today were already partially uplifted during Lago-Mare times (e.g., Benson and Rakic-El Bied, 1991; Roep et al., 1998; Fortuin and Krijgsman, 2003). They are dominated by mica schists and phyllites with more minor carbonates (Fig. 5A). To constrain the $^{87}Sr/^{86}Sr$ ratios of a hypothetical lake filling the Sorbas Basin which has a drainage basin with >50% mica schists and phyllites (labelled Sch; Fig. 5B), we assumed that these lithologies accounted for more than 50% of the dissolved Sr (Fig. 7A). The same threshold value is employed for all model outputs in the lagoonal scenario (Figs. 7C-E), where schists and phyllites are merged together with other similar lithologies carrying similar Sr concentration (Table 1; see Subsection 5.2 for insights). The Sr flux from mica schists and phyllites is decreased to 40% for the Nijar Basin and to 30% for the Vera Basin (Fig. 7B) to account for the higher volume of carbonates in the catchments of these two basins (Fig. 5A).

Using this approach the Sr dissolved in a hypothetical Messinian lake in the Sorbas Basin would have $^{87}Sr/^{86}Sr$ > 0.7100. Lower ratios are predicted for lakes in the Nijar (down to 0.7096) and Vera (down to 0.7092) basins. When Mediterranean water is added to the system of local rivers, the range of possible $^{87}Sr/^{86}Sr$ ratios in all basins is substantially lower, from 0.7088 to >0.7092 (Figs. 7C-E). Plotting the range of Sr isotope ratios measured on ostracods on top of the model results demonstrates that none of the predicted $^{87}Sr/^{86}Sr$ ratios for three endorheic lakes, one in each basin, overlaps with the measured values (Figs. 7A-B). Instead, measured and modelled $^{87}Sr/^{86}Sr$ ratios are in better agreement when Mediterranean Sr is mixed with the local riverine Sr (Figs. 7C-E).

6. Discussion

6.1. Causes and paleoenvironmental implications of the $^{87}Sr/^{86}Sr$ fingerprint of the Lago-Mare phase: is desiccation the only explanation?

The Lago-Mare scenario of non-marine sedimentation in a deep desiccated Mediterranean (here labelled to as "lacustrine scenario"; e.g., Ruggieri, 1967; Hsü et al., 1973; Cita et al., 1978; Benson and Rakic-El

Bied, 1991; Orszag-Sperber et al., 2000; Ryan, 2009; Maillard et al., 2014; Camerlenghi et al., 2019; Caruso et al., 2019; Kartveit et al., 2019; Madof et al., 2019; Raad et al., 2020) implies that each disconnected sub-basin had a unique base-level history and water chemistry. By contrast, the alternative scenario (i.e., "lagoonal scenario") envisages connection between sub-basins raised at elevations close to normal sea level by the same water mass filling the Mediterranean Basin (e.g., McCulloch and De Deckker, 1989; Roveri et al., 2014b, 2014c; Marzocchi et al., 2016; Vasiliev et al., 2017; García-Veigas et al., 2018; Grothe et al., 2020), which is expected to result in a more chemically-homogeneous water mass. Radiogenic strontium isotope ratios ($^{87}Sr/^{86}Sr$) reflect the source water inputs and can be used to discriminate between scenarios where the water sources have different $^{87}Sr/^{86}Sr$ ratios (e.g., Ingram and Sloan, 1992; Vonhof et al., 1998; Flecker et al., 2002; Doebbert et al., 2014). Strontium influx in the lacustrine scenario is derived from drainage within each catchment (Fig. 6A). The $^{87}Sr/^{86}Sr$ ratio of each water source is dependent upon the lithologies weathered in the watersheds and the Sr ratio of the resulting endorheic lake reflects all these inputs (Fig. 6A; Brenot, 2006; Bataille et al., 2012; Doebbert et al., 2014; Baddouh et al., 2016). In the lagoonal scenario, each marginal basin receives additional water from the Mediterranean (Fig. 6B), which in turn was supplied from the major peri-Mediterranean drainage systems (e.g., Nile, Rhone and Po; Griffin, 2002) plus the Eastern Paratethys (Flecker and Ellam, 2006; Krijgsman et al., 2010; Stoica et al., 2016; Grothe et al., 2020) and, possibly, the Atlantic (Manzi et al., 2009b; Vasiliev et al., 2017; García-Veigas et al., 2018; Grothe et al., 2020). Today, water masses strongly influenced by continental water but fully connected to ocean water (e.g., the Mediterranean and its coastal lagoons and estuaries) typically have an oceanic $^{87}Sr/^{86}Sr$ signature (Veizer, 1989; Flecker et al., 2002), because ocean water has a much higher (~100 times) Sr concentration (7.8 mg/l; Palmer and Edmond, 1992) than average river water (0.0780 mg/l; Palmer and Edmond, 1992). Because of the considerable difference in Sr concentration between marine and non-marine-derived Sr, a measurable deviation from global ocean $^{87}Sr/^{86}Sr$ ratios will only be achieved by a substantial increase in the source of non-marine Sr with respect to the marine-derived Sr (e.g., Ingram and Sloan, 1992). Numerical models applied to the Mediterranean Basin suggest that >25% of total water input needs to be fluvial discharge for the water mass to become more sensitive to the non-marine fluxes and evolve an $^{87}Sr/^{86}Sr$ away from the
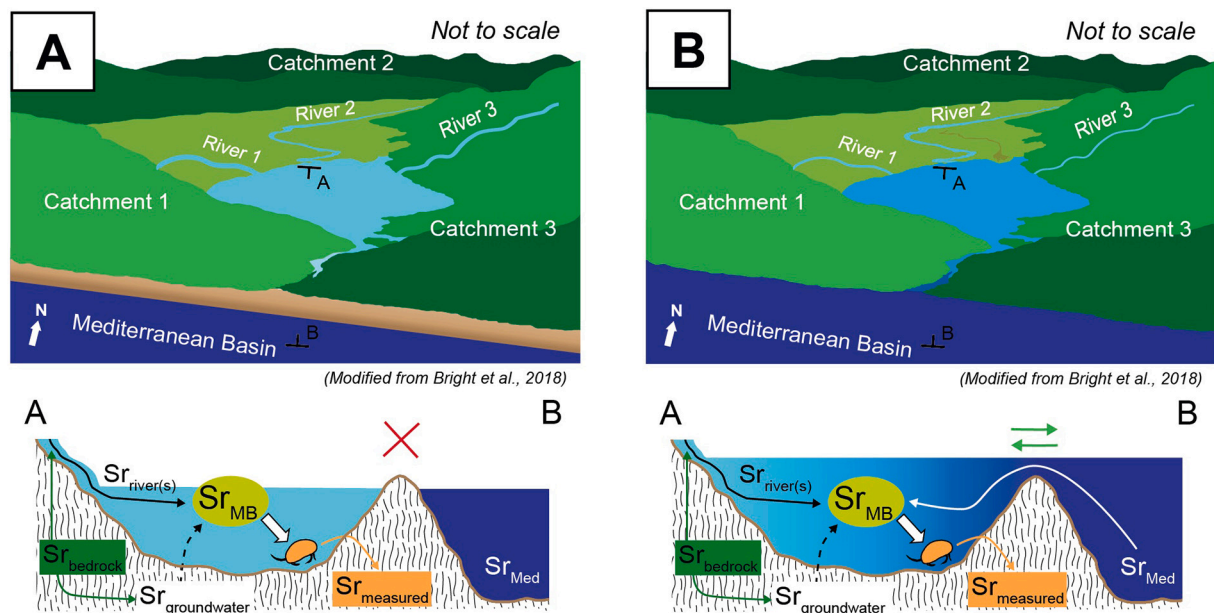

Fig. 6. Schematic presentation of the Sr cycle in a Mediterranean marginal basin (MB) disconnected from (A) and connected to (B) the Mediterranean water mass (modified from Bright et al., 2018).

ocean Sr isotope signature towards that of its contributing rivers (Topper et al., 2014).

Late Miocene ^{87}Sr/^{86}Sr data show that Mediterranean Sr isotope ratios progressively diverged from global ocean values during the MSC, before going back to follow the oceanic trend in the Pliocene (Fig. 4A). This trend has been interpreted as geochemical evidence for the restriction of Mediterranean-Atlantic connectivity accompanied by a proportional increase in low-salinity water supplied from Eastern Paratethys and/or major peri-Mediterranean rivers (Flecker et al., 2002; Flecker and Ellam, 2006; Vasiliev et al., 2010, 2017; Reghizzi et al., 2018; Grothe et al., 2020). The Lago-Mare phase yields the largest range of Sr isotope ratios during the MSC, from values higher than coeval ocean water (0.709027–0.709021; McArthur et al., 2012) to much lower ratios (down to ~0.7085; Fig. 4A). Most of the relatively high values (> 0.708750) come from marginal areas across the Mediterranean, while lower values are from the intermediate basin of Caltanissetta in Sicily (Grossi et al., 2015) and basinal locations accessed through DSDP drilling (Fig. 4A; McCulloch and De Deckker, 1989). Combined with the low salinity levels inferred from Lago-Mare fossils that resemble fauna dwelling in the Black Sea today (Bassetti et al., 2006; Gliozzi et al., 2007; Grossi et al., 2008; Stoica et al., 2016), the Lago-Mare Sr isotope dataset is consistent with negligible ocean water input and multiple isolated lakes fed by local streams.

The Lago-Mare stage is not the only time during the late Miocene when Sr isotope ratios drifted away from ratios within error of oceanic values (Fig. 4A). Some excursions have also been observed in pre-MSC marginal marine successions (Southern Turkey, Adriatic, Tyrrhenian Sea, Sorbas Basin; Flecker and Ellam, 1999, 2006; Flecker et al., 2002; Schildgen et al., 2014; Modestou et al., 2017; Reghizzi et al., 2017) and in equally marginal PLG sequences (Lugli et al., 2010; Schildgen et al., 2014; Reghizzi et al., 2018) (Fig. 4A). However, despite the non-oceanic ^{87}Sr/^{86}Sr ratio of some pre-MSC and PLG samples, the hypothesis of foraminifera dwelling and gypsum precipitating in endorheic lakes has never been contemplated because several lines of evidence indicated that a Mediterranean-Atlantic connection was present at that time (e.g., calcareous microplankton, marine sulfate of the gypsum, requirement of Atlantic salt for evaporite precipitation to take place; Krijgsman and Meijer, 2008; Lugli et al., 2010; Roveri et al., 2014a; García-Veigas et al., 2018). Although marine indicators in the Lago-Mare sediments (i.e., presence of gypsum with marine-like sulfate isotopic composition in the Balearic, Caltanissetta, Ionian, Levant and Polemi basins, Ricchiuto and McKenzie, 1978; Pierre, 1982; Pierre and Rouchy, 1990; Manzi et al., 2009b; García-Veigas et al., 2018; dwarf fauna of in situ-claimed planktonic foraminifera, Corbí and Soria, 2016; $\delta D_{n\text{-alkanes}}$ values in the range of normal marine isotopic values, Vasiliev et al., 2017) are scarcer than in pre-MSC and PLG successions and they are mixed with brackish water indicators (e.g., the same species of Black Sea ostracods everywhere in the Mediterranean; Gliozzi et al., 2007; Grossi et al., 2008; Stoica et al., 2016), these sedimentological, paleontological and geochemical indicators are also regarded as evidence of a Mediterranean water mass that was standing high and was periodically flooding the marginal basins during the Lago-Mare phase. As such, an influence of the Mediterranean water (and strontium) on marginal basins' sedimentary paleoenvironments, which would imply high sea level conditions, cannot be discarded a priori.

In a Mediterranean almost completely filled with oceanic water these deviations, typically towards lower ratios, require an increase in the proportion of non-marine ^{87}Sr/^{86}Sr contributing to the Mediterranean (achieved either by increasing freshwater input or declining oceanic input,) at a time when the oceanic input must have been close to the threshold at which non-marine Sr isotope ratios become analytically distinct from ocean water values. There are three controls on the proportion of fluvial and marine water sources in marginal marine settings:

1. The freshwater flux which, in the Mediterranean, is modulated on astronomical timescales by the African summer monsoon (Marzocchi et al., 2015) and Atlantic winter storms (Marzocchi et al., 2019).
2. The size of the gateway between the marginal basin and the main Mediterranean basin (Topper et al., 2011, 2014);
3. The density contrast between the marginal basin and the Mediterranean which drives exchange through the gateway (Topper et al., 2011). In the Mediterranean, density is mainly a function of salinity and reflects the interplay of the fresh and ocean water fluxes and net evaporation (Flecker et al., 2002). Modestou et al., (2017)'s study of the pre-MSC Sorbas Basin demonstrates that even without a reduction in gateway dimension, exchange is inhibited during periods of minimal density contrast, increasing the dominance of the fluvial contribution to the marginal basin sufficiently for the Sr isotope ratio to become analytically distinct from the coeval ocean value.

Correct interpretation of the Lago-Mare Sr isotope dataset as a whole therefore needs to take into account the distribution of the sites, climate variability, catchment changes and the gateways that link the marginal basins with the main Mediterranean as well as the Mediterranean-Atlantic gateway(s). In the case of SE Spain, the gateways that are known to have linked Sorbas, Nijar and Vera basins with each other and the Mediterranean up until the end of PLG deposition may also have had the potential to influence the Sr isotope ratios during the Lago-Mare phase.

6.2. Hydrological setting of SE Spain

In the Spanish basins, all the Lago-Mare Sr isotope data but one in Nijar plot outside the error interval of coeval ocean water values (Fig. 4B). This pattern of essentially non-oceanic Sr isotope ratios could, in principle, be consistent with the presence of three endorheic lakes, one in each sedimentary basin, with their Sr signature mostly driven by the geochemistry of their catchment-forming lithologies. This conclusion has already been suggested by some authors for the Sorbas (e.g., Aufgebauer and McCann, 2010) and Vera (Benson and Rakic-El Bied, 1991; Caruso et al., 2019) basins based on sedimentological and paleontological observations. Since calcium carbonate incorporates the Sr in the water from which it precipitates, if the Sorbas, Nijar and Vera basins were completely isolated lacustrine systems during the Lago-Mare phase, the ^{87}Sr/^{86}Sr ratios of the hosted ostracods are expected to fall within the range of ^{87}Sr/^{86}Sr values resulting from the mixing of only intrabasinal sources (i.e., rivers and groundwaters; Fig. 6A).

In the absence of knowledge about the chemistry of ancient river water, ^{87}Sr/^{86}Sr ratios of present-day rivers are typically used to reconstruct the paleohydrological regime of a water body at any specific time (e.g., Placzek et al., 2011; Doebbert et al., 2014). The strontium concentration and isotope ratio of the rivers feeding the Sorbas, Nijar and Vera basins during the Late Miocene are unknown and no measurements on modern rivers are available. However, because the isotopic composition of river water is a function of the isotopic composition of the lithologies in the watershed (Fig. 6; e.g., Brenot, 2006; Doebbert et al., 2014), some indicators of the paleofluvial geochemistry can be gleaned by analyzing the ^{87}Sr/^{86}Sr ratios of the rocks forming the sierras surrounding the basins (Figs. 1B, 5). Such an approach is justified by the lithological composition of both the coarse and fine-grained Lago-Mare facies in all three Spanish basins and some paleocurrent measurements (Fig. 2B; Benson and Rakic-El Bied, 1991; Roep et al., 1998; Fortuin and Krijgsman, 2003), which suggest that all the main lithologies forming the sierras today supplied clastics from areas partially emerged during the Lago-Mare phase. All these lithologies differ from each other in their isotopic compositions (Fig. 5B). Paleozoic para- and ortho-derived metamorphic rocks and Miocene volcanics are more radiogenic, with ^{87}Sr/^{86}Sr from 0.709691 up to 0.722831. In contrast, Triassic-Jurassic dolostones carry less radiogenic ^{87}Sr/^{86}Sr (average of 0.708612).

A closer look to the ^{87}Sr/^{86}Sr values measured on the Sorbas-Nijar-

Vera Lago-Mare ostracods reveals a trend of diminishing values from Sorbas (0.709066–0.709131) to Nijar (0.708835–0.709099) to Vera (0.708764–0.708813) (Fig. 4B). This trend indicates that from Sorbas to Vera, the water body filling each basin integrated more Sr from a lower radiogenic source. In the lacustrine scenario, rivers draining the Triassic-Jurassic carbonates could have provided dissolved Sr with a low radiogenic Sr signature. Given that these carbonates are more widespread in the catchment of Vera than in Nijar and they are very rare in Sorbas (Fig. 5A), the range of $^{87}Sr/^{86}Sr$ values measured on the Sorbas-Nijar-Vera ostracods might be the result of mixing of higher and lower intrabasinal water sources. However, modelling the $^{87}Sr/^{86}Sr$ resulting from the mixing of only intrabasinal rivers indicates that Sr provided by the Triassic-Jurassic carbonates would need to contribute >50% of the total Sr released into each basin in order to reproduce the $^{87}Sr/^{86}Sr$ isotope ratios measured on the ostracods (Figs. 7A-B). Although the exact fraction of Sr provided by each of the rivers is unknown, such a high contribution from carbonates is at odds with the outcropping geology in the catchments which are dominated by the other rock types (Fig. 5A), even adjusting for the higher solubility of carbonates as we have done here. Groundwater, which has been shown to make significant contributions to Sr budgets (e.g., Hart et al., 2004; Schildgen et al., 2014), is an alternative water source. The role of past groundwaters is difficult to assess (e.g., Placzek et al., 2011; Doebbert et al., 2014) and present-day measurements of the groundwater system of the region (e. g., Doebbert et al., 2014) are also lacking. However, geological cross-sections of the area (see Sanz de Galdeano and Santamaría-López, 2019 and references therein) reveal a subsurface geology similar to the

one exposed to subaerial weathering. This means that if a substantial groundwater network was present in the region during the Lago-Mare time, it was adding to the hydrologic system isotopic compositions and concentrations similar to the one provided by surface water.

The results of modelling the lacustrine Sr isotope ratios of the three Spanish basins based on their catchment geology suggest that these would have been as low as 0.7092 in Vera, 0.7096 in Nijar (Fig. 7B) and 0.7100 in Sorbas (Fig. 7A), all values substantially higher than those measured on the ostracods (Fig. 4B; Figs. 7A-B). This mismatch between the $^{87}Sr/^{86}Sr$ values measured on ostracods and $^{87}Sr/^{86}Sr$ ratios expected from the lake water implies that, to satisfy the mixing relationships, there was an additional contribution of less radiogenic water during deposition of the Lago-Mare carbonates in Sorbas and mudstones in Nijar and Vera.

One possibility is that the source of less radiogenic Sr was the dissolution of pre-existing evaporites in the basins, which is a process observed to have played a major role in the formation of the late Tortonian gypsum deposits of the internal Betic basins (Fig. 1A; e.g., Campo Coy, Lorca and Fortuna; Ortí et al., 2014; García-Veigas et al., 2019; Artiaga et al., 2020), and/or Stage 1 brines remained in the basins after their disconnection from the Mediterranean during Stage 2. However, Stage 1 gypsum has Sr isotope ratios similar to coeval sea water (Reghizzi et al., 2018) and this is too high to depress the fluvial signal to the Sr isotope ratios measured on Lago-Mare ostracods. Stage 2 halite, which potentially have sufficiently low $^{87}Sr/^{86}Sr$ to draw modelled values down to the ostracod values (Fig. 4A), has not been found in these basins and so cannot be a dissolved source of low Sr isotope water during
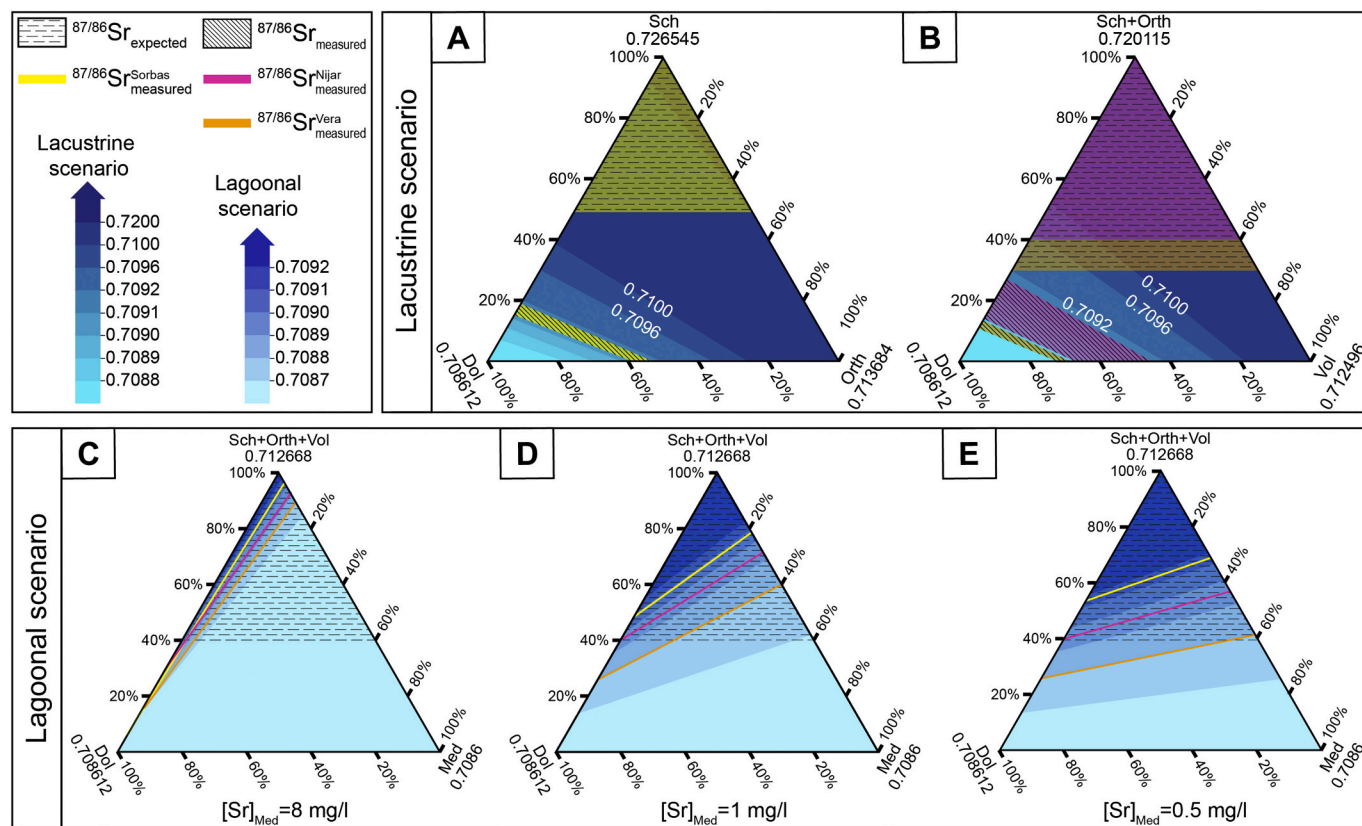

Fig. 7. Ternary diagrams of the $^{87}Sr/^{86}Sr$ isotope ratios modelled for both the lacustrine (A, B) and lagoonal (C, D, E) scenarios. End member compositions and Sr concentrations are average values for the specific rock types in the catchment as shown in Fig. 5B and Table 1. These are schist and phyllites (Sch), ortho-derived metamorphic rocks (Orth), volcanic rocks (Vol) and dolostones (Dol). The Mediterranean Sr isotope ratio employed (i.e., 0.7086) corresponds to the midpoint value of the range of values for Lago-Mare Sr ratios derived from intermediate and deep Mediterranean basins (Fig. 4A; Supplementary Material S1). The Sr concentration of Mediterranean water used to calculate the $^{87}Sr/^{86}Sr$ isofields are 8 mg/l (C), 1 mg/l (D) and 0.5 mg/l (E). The dashed areas of the ternary diagrams highlight the range of Sr ratios anticipated from the outcropping geology shown in Fig. 5A for the lacustrine and lagoonal scenarios. The range of $^{87}Sr/^{86}Sr$ ratios measured for each basin (see Fig. 4B) is also plotted to facilitate the comparison with the model outputs.

Stage 3. If local streams, groundwater and Stage 1 evaporites/water cannot account for the Sr isotope ratios measured on Lago-Mare ostracods, the only left source of low radiogenic Sr is the Mediterranean water mass during Stage 3. For it to have contributed to these marginal basins, its base level must have been at the level of these marginal Spanish basins during the Lago-Mare.

6.3. Sr isotope consequences of the lagoonal scenario for the Lago-Mare story

The main challenge to modelling the input of Mediterranean water into the Spanish marginal basins is its compositional uncertainty during the Lago-Mare. The literature contains interpretations of Mediterranean water in the Lago-Mare as being totally marine (e.g., Carnevale et al., 2018) or brackish (McCulloch and De Deckker, 1989; Roveri et al., 2008a) or density-stratified (Roveri et al., 2014c; Marzocchi et al., 2016; Vasiliev et al., 2017; García-Veigas et al., 2018) with a hypersaline brine of unknown composition possibly resting at the bottom (Marzocchi et al., 2016; Gvirtzman et al., 2017; García-Veigas et al., 2018). Each compositional interpretation involves different contributing water sources (fluvial, epi-continental and oceanic), and each therefore suggests a different Mediterranean $^{87}Sr/^{86}Sr$ and [Sr]. Fortunately, well-preserved in situ Lago Mare ostracods (e.g., Iaccarino and Bossio, 1999; Grossi et al., 2015) are present in more central Mediterranean basins like the intermediate basin of Caltanissetta (Grossi et al., 2015) and the deeper Balearic and Levantine basins (e.g., McCulloch and De Deckker, 1989; Iaccarino and Bossio, 1999). Regardless of the salinity of the Mediterranean water mass at the time, the $^{87}Sr/^{86}Sr$ of these central basin ostracods provides us with an indication of its $^{87}Sr/^{86}Sr$ fingerprint. During the Lago-Mare, the Sr isotope ratio of the central Mediterranean basins was ~0.7085–0.7087 (Fig. 4A; McCulloch and De Deckker, 1989; Grossi et al., 2015), low relative to the measured values in the Spanish marginal basins.

More challenging is obtaining a reliable value for strontium concentration, which under normal circumstances varies with salinity such that [Sr] equal to the modern seawater (i.e., 8 mg/l; Veizer, 1989) is around two orders of magnitude greater than that of global river water (0.0780 mg/l; Palmer and Edmond, 1992). However, given that the latest Miocene Mediterranean record contains fossils that indicate it was not entirely marine and gypsum intervals indicating higher salt concentrations than purely fresh water, it is likely that Sr concentration during the Lago-Mare lays somewhere between these two end-member values.

To evaluate the impact of this uncertainty, we modelled the Mediterranean input with a range of different Sr concentrations (Figs. 7C-E). These results indicate that the combination of Spanish catchment rocks and Mediterranean-derived water can reproduce the $^{87}Sr/^{86}Sr$ ratios of the Spanish ostracods in both the extreme (and unlikely) scenarios of a Mediterranean water mass carrying a present-day like Sr concentration (Fig. 7C) or an extremely low, fluvial-like Sr concentration (Fig. 7E). The difference among the scenarios resides in the quantity of Mediterranean water required to explain a fixed $^{87}Sr/^{86}Sr$ value, which varies from <20% assuming a sea water [Sr] (Fig. 7C) up to 60% for the Vera results where the [Sr] approaches fresh-water concentrations (Fig. 7E). These modelling results are therefore compatible with a scenario in which the main Mediterranean Basin (or at least its western domain) was sufficiently full to allow it to contribute with water to these marginal Spanish basins during the Lago-Mare subaqueous sedimentation. This is consistent with published stratigraphic and sedimentological arguments concerning the Sorbas and Nijar basins (Fortuin and Krijgsman, 2003; Omodeo Salé et al., 2012). It is also compatible with the homogeneity of the ostracod assemblages, not only among Spanish basins (including Malaga, Guerra-Merchán et al., 2010), but throughout the Mediterranean and the Eastern Paratethys, which points to a water body stretching from the Alborán margins as far as Eastern Europe (Stoica et al., 2016; Van Baak et al., 2016). This conclusion counters the hypothesis that

these Spanish basins persisted as isolated lakes throughout the Lago-Mare phase until the transition to the Zanclean (Aufgebauer and McCann, 2010; Caruso et al., 2019).

One further consideration is whether this scenario is compatible with seismic-based studies of the western Mediterranean's offshore record. Gypsum-bearing seismic units with different seismic facies and erosional base and top surfaces have been recognized in different intermediate and deep subbasins. The facies variability has been interpreted as being indicative of unique hydrological settings for each isolated subbasin, with the erosional surfaces ascribed to subaerial erosion during exposure periods (e.g., Maillard and Mauffret, 2006; Maillard et al., 2014; Thinon et al., 2016; Lymer et al., 2018; Raad et al., 2020). These conclusions are clearly at odds with a Stage 3 scenario of a near full Mediterranean, but alternatives to these interpretations are not provided. However, recent research suggests that these seismic features may be open to alternative explanations. Deep erosional surfaces, for example, are not only formed as a consequence of subaerial exposure, but can also form in deep-water well-stratified settings (Gvirtzman et al., 2017; Kirkham et al., 2020). Lateral facies changes, which are common in marginal, gypsum-precipitating settings (Piedmont Basin, Dela Pierre et al., 201 l; Po Plain-Adriatic Foredeep, Ghielmi et al., 2013; Northern Apennines, Roveri et al., 2001; Caltanissetta Basin, Roveri et al., 2008b), may result from precession-controlled vertical oscillations of the chemocline in a deeper, stratified water column (e.g., Sabino et al., 2020). In addition, gypsum precipitating in endorheic, freshwater-fed basins is inconsistent with the marine isotopic signature of sulfate recovered from deep-water sites (e.g., Pierre and Fontes, 1978; Ricchiuto and McKenzie, 1978; Pierre, 1982; Pierre and Rouchy, 1990; García-Veigas et al., 2018).

It therefore seems possible to reconcile offshore with high Mediterranean water level conditions during the final stage of the MSC. In view of the foregoing, we stress that alternatives should be considered in future studies targeting/modelling the deep record and discussed in light of the observations/conclusions provided from the outcrops.

6.4. Was the Mediterranean base-level fluctuating with precessional periodicity?

This compilation of Sr isotope measurements on ostracods shows that a trend exists in the $^{87}Sr/^{86}Sr$ data of the Spanish basins (i.e., Sorbas shows more radiogenic values than Vera and with Nijar in between; Fig. 4B). Mass-balance calculations show that for a constant value of Mediterranean Sr concentration the percentage of Mediterranean water required to explain the measured Sr isotope ratios increases from Sorbas to Nijar and to Vera (Figs. 7C-E). This is broadly compatible with their spatial relationship to the Mediterranean, with the Sorbas Basin located more landward relative to the Nijar and Vera basins. However, both the sedimentary successions and the Sr data (Fig. 4B) suggest that the amount of Mediterranean water entering the basins also varied through time (Fig. 8).

The alternation of continental conglomerate-sandstone and lagoonal mudstones of the Upper Mb. of the Feos Fm. in the Nijar Basin indicates that base-level changes were controlling the sedimentation during the Lago-Mare phase, possibly with precessional periodicity (Fortuin and Krijgsman, 2003; Omodeo Salé et al., 2012). Since Mediterranean water contributed to the hydrology of the lagoonal environment (Figs. 7C-E), it follows that Mediterranean fluctuations in water level are likely to have mirrored and driven the base-level changes seen in the Nijar Basin. During the arid phase of the cycle (i.e., precession maxima-insolation minima) fluvial conglomerates were being deposited by the intra-basinal rivers (Fig. 2B). This means that the Nijar Basin could not have been receiving Mediterranean water during this phase (Fig. 8A) at least in the northern area of the basin, where the studied sections are located (Fig. 1B). Lagoonal deposition in Nijar occurred in the humid phase of the precessional cycle (Fig. 2B), therefore indicating that a base-level rise occurred at the conglomerate-mudstone transition. The uppermost two mudstone horizons in the astronomically-tuned Barranco de los
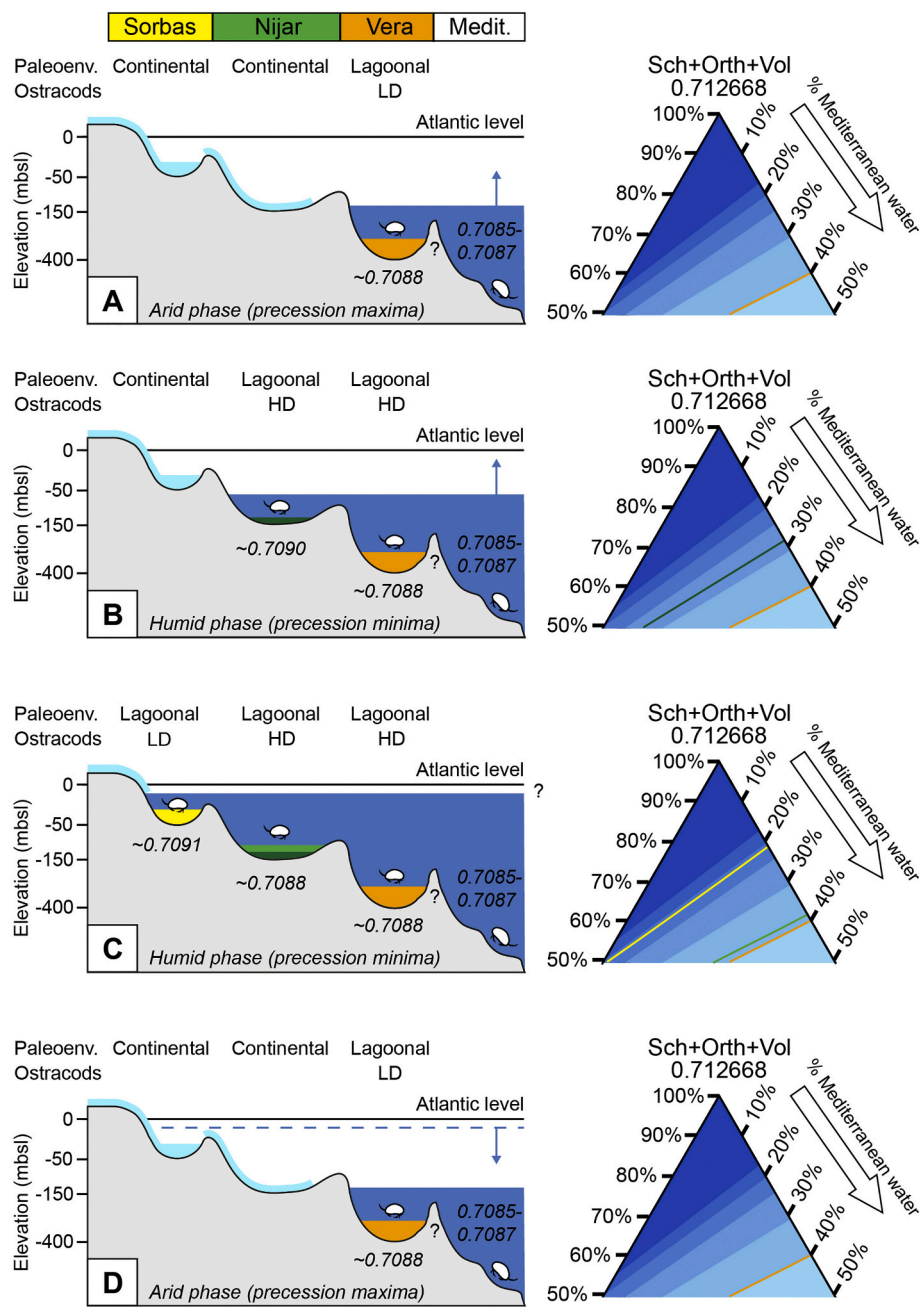
Fig. 8. Schematic illustration of the paleohydrological evolution of the Sorbas (yellow), Nijar (light and dark green) and Vera (orange) basins during a precessional cycle of the Lago-Mare phase. A) Fluviatile accumulation occur in Nijar and Sorbas during arid phases at precession maxima (insolation minima), while the Mediterranean base-level is at its minimum and only enters the deeper Vera Basin. B) Orbitally-driven fluctuations of the Mediterranean base-level cause the transition, in Nijar, from continental to lagoonal conditions during humid phases at precession minima (insolation maxima). Water depth and ostracod species diversity increase in Vera. Continental conditions persist in Sorbas. C) Before entering the arid conditions again (D), the Mediterranean base-level reach the climax. Ostracods diversity further increase in Vera and Nijar and Sr isotope ratios among the two basins are leveled. Mediterranean waters penetrate in the Sorbas Basin, interrupting the fluviatile sedimentation and bringing few species of ostracods. The triangular plot on the right side (portion of Fig. 7D) aims to visualize the different amount of water necessary to explain the Sr data of each basin. The dark green line corresponds to the Sr data from the base of the mudstone horizons in the Barranco de los Castellones section (see Fig. 2B). Light green like corresponds to the Sr data from the top of the mudstone horizons in the Barranco de los Castellones section (see Fig. 2B). Ostracods data are from Roep and Van Harten (1979) for Sorbas, Bassetti et al. (2006) for Nijar and Stoica et al. (2016) for Vera. LD: Low diversity; HD = High diversity. The depth scale is from the depth data from the base of the Pliocene (see Subsection 6.4 for explanation and references). (For interpretation of the references to colour in this figure legend, the reader is referred to the web version of this article.)

Castellones section show that mudstone deposition may have been accompanied by a systematic change in the $^{87}Sr/^{86}Sr$ values (Fig. 4B) where the higher ratios, indicative of a more fluvially-dominated signal, come from immediately above the transition from fluvial conglomerates to lacustrine pelitic sedimentation (Fig. 2B). This sedimentary transition is interpreted as the onset of a transgression in each cycle (Fortuin and Krijgsman, 2003; Omodeo Salé et al., 2012) and it is therefore a moment at which only a limited amount of Mediterranean water was entering the basin (Fig. 8B). The less radiogenic values, suggesting a larger contribution from the Mediterranean, occur just below the transition to the overlying continental facies of the next precession cycle (Fig. 8C), when the basin, before emptying again (Fig. 8D), was more replenished. A dynamic contribution of Mediterranean water also seems the most logical way to explain the episodic appearance of lagoonal carbonates in the otherwise continental Sorbas Basin (Figs. 2B, 3C). Our observation that Sr values in Sorbas cannot be explained by simple mixing of local

source water suggests that a short-lived Sorbas-Mediterranean connection was episodically established via one, if not both, of the two neighbouring basins during highest water level intervals (Fig. 8C).

A fluctuating Mediterranean base-level may also be mirrored in the ostracod record which, like strontium, correlates closely with the sedimentary facies. In the Vera and Nijar basins, a low-diversity assemblage mainly dominated by the euryhaline and shallow water *Cyprideis* sp. and indicative of more fluctuating environmental conditions characterizes the basal mudstones (Figs. 8A-B), while at the top a plethora of more stenohaline and deeper water species with Paratethyan affinity and indicative of a more stable environment occurs (Figs. 8B-C; Bassetti et al., 2006; Stoica et al., 2016; Caruso et al., 2019). This trend suggests that during the lowstand phases in each of the two basins (Figs. 8A-B) physical and chemical conditions were only suitable for species more tolerant to harsh and fluctuating environmental conditions, while only during the highstands (Figs. 8B-C) more favorable and stable

environmental conditions required by the Paratethyan species were created. The full Paratethyan contingent apparently never reached the Sorbas Basin, where only few opportunistic species are found (Roep and Van Harten, 1979; Aufgebauer and McCann, 2010). The lower diversity with respect to the adjacent basins suggests that environmental parameters in Sorbas did not evolve sufficiently favorable conditions for the Black Sea ostracods to flourish, possibly because Mediterranean incursions and retreats happened only over a relatively short period of time (not quantifiable with our dataset). This is in agreement with the ephemeral character of the lagoonal environment suggested by the intercalation of thin and spatially-confined limestones in a dominantly continental succession (Figs. 2B, 3C; Aufgebauer and McCann, 2010).

The entrance of Mediterranean water in the few tens of meters deep Sorbas Basin (Roveri et al., 2019) means that Mediterranean base-level was standing slightly beneath if not at the level of the Atlantic during the highstand phases (Fig. 8C). Conversely, the deepest Vera Basin provides us with an idea of the lower limit of the fluctuations of the base level. The persistence of fine sedimentation in Vera through the Lago-Mare phase (Fig. 2A) and rather constant vertical trend of the Sr isotope ratio (Fig. 4B) indicate that even though the base level of the Mediterranean has changed over time, the amount of water delivered to the basin during the lowstand (Fig. 8A) and highstand (Fig. 8C) phases did not change enough to expose the basin subaerially, to trigger a facies change or to shift the Sr signature of the lagoon towards more local sources' values as is seen in Nijar. This means that the Mediterranean base-level did not drop beneath the bottom of the Vera Basin, estimated to stand at 400–500 m at the base of the Pliocene (Ott d'Estevou et al., 1990), or beneath its sill height if there was one. Putting together all these sedimentological and geochemical constrains, we suggest that (western) Mediterranean base-level during the Lago-Mare was high, probably close to the Atlantic level and that it fluctuated by a maximum of ~400 ± 100 m per precession cycle. The inferred precessional character of the lithological cyclicity (Krijgsman et al., 2001; Fortuin and Krijgsman, 2003; Roveri et al., 2009; Omodeo Salé et al., 2012) suggests that an orbitally-forced climatic driver lies behind such variations.

6.5. Future direction: merging together marginal and deep basins observations

Considering that the Mediterranean Basin was subdivided in a complex system of variably deep sub-basins separated by physical thresholds of largely unknown depths (Amadori et al., 2018; Camerlenghi et al., 2019), a high and fluctuating Mediterranean base-level cannot be straightforwardly extrapolated to the whole Mediterranean on the basis of data exclusively from the far western end. A high Mediterranean base-level during Lago-Mare has always been regarded at odds with Mediterranean-wide seismic (e.g., Maillard and Mauffret, 2006; Maillard et al., 2014; Thinon et al., 2016; Lymer et al., 2018; Amadori et al., 2018; Micallef et al., 2018, 2019; Camerlenghi et al., 2019; Kartveit et al., 2019; Madof et al., 2019; Raad et al., 2020; Spatola et al., 2020) and modelling (García-Castellanos et al., 2020 and references therein) interpretations, which mostly point to a low Mediterranean water level in the latest Messinian and, as a consequence, to a sudden and catastrophic restoration of high sea-level conditions at the Mio-Pliocene boundary. However, we showed that some data, mostly from the margins (^{87}Sr/^{86}Sr ratios and W-E homogeneity of Paratethyan ostracod assemblages) but also from deeper, offshore settings (sulfate isotopes of the Upper Evaporites units) are not explainable in the lacustrine scenarios, while arguments apparently in favor of it may have alternative explanations that, however, are rarely addressed and discussed. Furthermore, a full Mediterranean base-level fluctuating hundreds of meters in a Mediterranean compartmentalized into sub-basins of variable depth and area do not necessarily imply that marginal and basinal observations are mutually exclusive, with the erosional features and fluvial deposits imaged by the seismic that may have been formed during lowstand phases. Waiting for the success of the on-going

Mediterranean drilling proposals (DEMISE, DREAM and IMMAGE; Camerlenghi and Aloisi, 2020) that would provide the Messinian community with cores potentially suitable to solve the onshore-offshore correlation riddle, we suggest that future studies targeting the deep basinal successions should examine whether base-level fluctuations of hundreds of meters in a full Mediterranean could reproduce the sedimentological, paleontological and geochemical features observed in existing seismic profiles and wells.

7. Conclusions

Compiled ^{87}Sr/^{86}Sr data from the ostracods that inhabited the adjoining Sorbas, Nijar and Vera basins during the Lago-Mare along with strontium mass-balancing modelling and existing sedimentological and paleontological data shed new light on the terminal Lago-Mare phase of the MSC. The ^{87}Sr/^{86}Sr ratios from these three Spanish basins cannot be explained by an environment shaped only by local river and groundwater inputs, or with Mediterranean Stage 1 Sr retained in the system after the isolation of the basins during Stage 2 or in solution into groundwaters draining buried PLG deposits, but require an additional external water source with a low radiogenic Sr isotope ratio. Instead, the measured isotopic data are reproduced when the Mediterranean is added to the hydrologic system. This is compatible with a near full Mediterranean during the Lago-Mare rather than the hypothesis that these Spanish basins were isolated lakes perched above a deeply desiccated Mediterranean. Combined analysis of sedimentological, paleontological and geochemical data suggest that Mediterranean base-level during the Lago-Mare fluctuated by several hundred meters with precessional periodicity, with the lowstand reached during the arid phase of the cycle (precession maxima-insolation minima) and the highstand reached during the humid phase (precession minima-insolation maxima). Consequently, we conclude that sedimentation in the marginal Spanish basins (and in other marginal Mediterranean systems) during the wet precessional phases of the Lago-Mare stage occurred in a relatively full Mediterranean.

Declaration of Competing Interest

The authors whose names are listed immediately below certify that they have NO affiliations with or involvement in any organization or entity with any financial interest (such as honoraria; educational grants; participation in speakers' bureaus; membership, employment, consultancies, stock ownership, or other equity interest; and expert testimony or patent-licensing arrangements), or non-financial interest (such as personal or professional relationships, affiliations, knowledge or beliefs) in the subject matter or materials discussed in this manuscript.

Acknowledgements

Appendix A. Supplementary data

Supplementary data to this article can be found online at https://doi.org/10.1016/j.palaeo.2020.110139.

References

Aguirre, J., 1998. El Plioceno del SE de la Peninsula Iberica (provincia de Almeria). Sintesis estratigrafica, sedimentaria, bioestratigrafica y paleogeografica. Rev. Soc. Geol. Esp. 11, 295–315.

Aguirre, J., Sánchez-Almazo, I.M., 2004. The Messinian post-evaporitic deposits of the Gafares area (Almeria-Nijar basin, SE Spain). A new view of the "Lago-Mare" facies. Sediment. Geol. 168, 71–95.

Albarède, F., Michard, A., 1987. Evidence for slowly changing $^{87}Sr/^{86}Sr$ in runoff from freshwater limestones of southern France. Chem. Geol. 64, 55–65.

Amadori, C., García-Castellanos, D., Toscani, G., Sternai, P., Fantoni, R., Ghielmi, M., Di Giulio, A., 2018. Restored topography of the Po Plain-Northern Adriatic region during the Messinian base level drop—Implications for the physiography and compartmentalization of the palaeo-Mediterranean basin. Basin Res. 30 (6), 1247–1263. https://doi.org/10.1111/bre.12302.

Arribas Jr., A., Cunningham, C.G., McKee, E.H., Rye, R.O., Rytuba, J.J., Tosdal, R.T., Wasserman, M.D., Aoki, M., 1995. Compilation of sample preparation and analytical method and results of chemicals, isotopic, and fluid inclusion annalyses, Rodalquilar Ar alunite deposit Spain. In: U.S. Geological Survey Open-File Report 95–221 (33 pp.).

Artiaga, D., García-Veigas, J., Gibert, L., Soria Mingorance, J.M., 2020. The late Miocene Campo Coy gypsum (Eastern Betics, Spain). Geogaceta 67, 64–67.

Aufgebauer, A., McCann, T., 2010. Messinian to Pliocene transition in the deep part of the Sorbas Basin, SE Spain-a new description of the depositional environment during the Messinian Salinity Crisis. Neues Jahrbuch für Geologie und Paläontologie-Abhandlungen 259 (2), 177–195.

Baddouh, M.B., Meyers, S.R., Carroll, A.R., Beard, B.L., Johnson, C.M., 2016. Lacustrine $^{87}Sr/^{86}Sr$ as a tracer to reconstruct Milankovitch forcing of the Eocene hydrologic cycle. Earth Planet. Sci. Lett. 448, 62–68.

Bassetti, M.A., Miculan, P., Sierro, F.J., 2006. Evolution of depositional environments after the end of Messinian Salinity Crisis in Nijar basin (SE Betic Cordillera). Sediment. Geol. 188-189, 279–295.

Bataille, C.P., Laffoon, J., Bowen, G.J., 2012. Mapping multiple source effects on the strontium isotopic signatures of ecosystems from the circum-Caribbean region. Ecosphere 3 (12), 1–24.

Beets, C.J., 1991. $^{87}Sr/^{86}Sr$ dating of coralline algal limestones and its implications for the tectono-stratigraphic evolution of the eastern Prebetic (Spain). Sediment. Geol. 78, 233–250.

Benson, R.H., 1978. The paleoecology of the ostracods of DSDP Leg 42A. In: Hsu, K., Montadert, L. (Eds.), Initial Reports of the Deep-Sea Drilling Project 42. U.S. Government Printing Office, Washington, pp. 777–787.

Ben-Moshe, L., Ben-Avraham, Z., Enzel, Y., Schattner, U., 2020. Estimating drawdown magnitudes of the Mediterranean Sea in the Levant basin during the Lago Mare stage of the Messinian Salinity Crisis. Marine Geology 0, 106215. https://doi.org/10.1007/s10640-008-9233-9.

Benson, R.H., Rakic-El Bied, K., 1991. The Messinian parastratotype at Cuevas de Almanzora, Vera Basin, SE Spain; refutation of the deep-basin, shallow-water hypothesis? Micropaleontology 37 (3), 289–302.

Bickle, M.J., Harris, N.B.W., Bunbury, J.M., Chapman, H.J., Fairchild, I.J., Ahmad, T., 2001. Controls on the 87Sr/86Sr ratio of carbonates in the Garhwal Himalaya, headwaters of the Ganges. J. Geol. 109 (6), 737–753.

Blanc-Valleron, M.-M., Rouchy, J.-M., Pierre, C., Badaut-Trauth, D., Schuler, M., 1998. Evidence of Messinian non-marine deposition at Site 968 (Cyprus Lower Slope). In: Robertson, A.H.F., Emeis, K.-C., Richter, C., Camerlenghi, A. (Eds.), Proc. ODP, Sci. Results, vol. 160. Ocean Drilling Program, College Station, TX, pp. 437–445.

Bonaduce, G., Sgarrella, F., 1999. Paleoecological Interpretation of the Latest Messinian Sediments from Southern Sicily (Italy). Mem. Soc. Geol. Ital, LIV, pp. 83–92.

Bourillot, R., Vennin, E., Rouchy, J.M., Blanc-Valleron, M.M., Caruso, A., Durlet, C., 2010. The end of the Messinian Salinity Crisis in the western Mediterranean: insights from the carbonate platforms of South-Eastern Spain. Sediment. Geol. 229 (4), 224–253.

Brachert, T.C., Krautworst, U.M.R., Steuckrad, O.M., 2002. Tectono-climatic evolution of a Neogene intramontane basin (Late Miocene Carboneras subbasin, Southeast Spain): revelations from basin mapping and biofacies analysis. Basin Res. 14, 503–521.

Braga, J.C., Martín, J.M., Riding, R., Aguirre, J., Sánchez-Almazo, I.M., Dinarès-Turell, J., 2006. Testing models for the Messinian salinity crisis: the Messinian record in Almería, SE Spain. Sediment. Geol. 188, 131–154.

Brass, G.W., 1976. The variation of the marine $^{87}Sr/^{86}Sr$ ratio during Phanerozoic time: interpretation using a flux model. Geochim. Cosmochim. Acta 40 (7), 721–730.

Brenot, A., 2006. Origine de l'eau et Des Éléments Dissous Par traçage Isotopique (H, O, S,Mg, Sr) Sur le Bassin Amont de La Moselle PhD thesis INPL - ENSG - CRPG (360 pp.).

Bright, J., Cohen, A.S., Dettman, D.L., Pearthree, P.A., 2018. Freshwater plumes and brackish lakes: Integrated microfossil and OC-Sr isotopic evidence from the late Miocene and early Pliocene Bouse Formation (California-Arizona) supports a lake overflow model for the integration of the lower Colorado River corridor. Geosphere 14 (4), 1875–1911.

Camerlenghi, A., Aloisi, V., 2020. Uncovering the Mediterranean Salt Giant (MEDSALT)-Scientific Networking as Incubator of Cross-disciplinary Research in Earth Sciences. Eur. Rev. 28 (1), 40–61.

Camerlenghi, A., Ben Del, A., Hübscher, C., Forlin, E., Geletti, R., Brancatelli, G., Micallef, A., Saule, M., Facchin, L., 2019. Seismic markers of the Messinian salinity crisis in the deep Ionian Basin. Basin Res. 00, 1–23.

Capella, W., Matenco, L., Dmitrieva, E., Roest, W.M., Hessels, S., Hssain, M., Chakor-Alami, A., Sierro, F.J., Krijgsman, W., 2017. Thick-skinned tectonics closing the Rifian Corridor. Tectonophysics 710, 249–265.

Capella, W., Barhoun, N., Flecker, R., Hilgen, F.J., Kouwenhoven, T.E., Matenco, L., Sierro, F.J., Tulbure, M., Yousfi, Z., Krijgsman, W., 2018. Paleogeographic evolution of the Late Miocene Rifian Corridor (Morocco): reconstructions from surface and subsurface data. Earth-Sci. Rev. 180, 37–59.

Carnevale, G., Dela Pierre, F., Natalicchio, M., Landini, W., 2018. Fossil marine fishes and the 'Lago Mare' event: has the Mediterranean ever transformed into a brackish lake? Newsl. Stratigr. 51 (1), 57–72.

Caruso, A., Blanc-Valleron, M.M., Da Prato, S., Pierre, C., Rouchy, J.M., 2019. The late Messinian "Lago-Mare" event and the Zanclean Reflooding in the Mediterranean Sea: new insights from the Cuevas del Almanzora section (Vera Basin, South-Eastern Spain). Earth Sci. Rev. 102993.

Castradori, D., 1998. Calcareous nannofossils in the basal Zanclean of the Eastern Mediterranean Sea: Remarks on palaeoceanography and sapropel formation. In: Robertson, A.H.F., Emeis, K.C., Richter, C., Camerlenghi, A. (Eds.), Proceedings of the Ocean Drilling Program, Scientific Results 160. US Government Printing Office, Washington, pp. 113–123.

Cita, M.B., Wright, R.C., Ryan, W.F.B., Longinelli, A., 1978. Messinian paleoenvironments. In: Ryan, W.B.F., Hsü, K.J., et al. (Eds.), Init. Rep. Deep Sea Drill. Proj, vol. 42A. U.S. Government Printing Office, Washington, pp. 1003–1035, 1.

Conticelli, S., Guarnieri, L., Farinelli, A., Mattei, M., Avanzinelli, R., Bianchini, G., Boari, E., Tommasini, S., Tiepolo, M., Prelevic, D., Venturelli, G., 2009. Trace elements and Sr-Nd-Pb isotopes of K-rich, shoshonitic, and calc-alkaline magmatism of the Western Mediterranean Region: genesis of ultrapotassic to calc-alkaline magmatic associations in a post-collisional geodynamic setting. Lithos 107 (1–2), 68–92.

Corbí, H., Soria, J.M., 2016. Late Miocene–early Pliocene planktonic foraminifer event-stratigraphy of the Bajo Segura basin: a complete record of the western Mediterranean. Mar. Pet. Geol. 77, 1010–1027. https://doi.org/10.1016/j.marpetgeo.2016.08.004.

Corbí, H., Lancis, C., García-García, F., Pina, J.A., Soria, J.M., Tent-Manclús, J.E., Viseras, C., 2012. Updating the marine biostratigraphy of the Granada Basin (central Betic Cordillera). Insight for the Late Miocene paleogeographic evolution of the Atlantic–Mediterranean seaway. Geobios 45 (3), 249–263.

Cosentino, D., Gliozzi, E., Pipponzi, G., 2007. The late Messinian Lago-Mare episode in the Mediterranean Basin: preliminary report on the occurrence of Paratethyan ostracod fauna from Central Crete (Greece). Geobios 40 (3), 339–349.

Dela Pierre, F., Bernardi, E., Cavagna, S., Clari, P., Gennari, R., Irace, A., Lozar, F., Lugli, S., Manzi, V., Natalicchio, M., Roveri, M., Violanti, D., 2011. The record of the Messinian salinity crisis in the Tertiary Piedmont Basin (NW Italy): the Alba section revisited. Paleogeogr. Paleoclimatol. Paleoecol. 310, 238–255.

Doebbert, A.C., Johnson, C.M., Carroll, A.R., Beard, B.L., Pietras, J.T., Carson, M.R., Norsted, B., Throckmorton, L.A., 2014. Controls on Sr isotopic evolution in lacustrine systems: Eocene green river formation, Wyoming. Chem. Geol. 380, 172–189.

Dronkert, H., 1976. Late Miocene evaporites in the Sorbas Basin and adjoining areas. Mem. Soc. Geol. Ital. 16, 341–361.

Evans, N.P., Turchyn, A.V., Gázquez, F., Bontognali, R.R., Chapman, H.J., Hodell, D.A., 2015. Coupled measurements of $\delta^{18}O$ and δD of hydration water and salinity of fluid inclusions in gypsum from the Messinian Yesares Member, Sorbas Basin (SE Spain). Earth Planet. Sci. Lett. 430, 499–510.

Flecker, R., Ellam, R.M., 1999. Distinguishing climatic and tectonic signals in the sedimentary successions of marginal basins using Sr isotopes: an example from the Messinian salinity crisis, Eastern Mediterranean. J. Geol. Soc. 156 (4), 847–854.

Flecker, R., Ellam, R.M., 2006. Identifying Late Miocene episodes of connection and isolation in the Mediterranean-Paratethyan realm using Sr isotopes. Sediment. Geol. 188-189, 189–203.

Flecker, R., de Villiers, S., Ellam, R.M., 2002. Modelling the effect of evaporation on the salinity-$^{87}Sr/^{86}Sr$ relationship in modern and ancient marginal-marine systems: the Mediterranean Messinian Salinity Crisis. Earth Planet. Sci. Lett. 203, 221–233.

Flecker, R., Krijgsman, W., Capella, W., de Castro Martíns, C., Dmitrieva, E., Mayser, J.P., Marzocchi, A., Modestu, S., Ochoa, D., Simon, D., Tulbure, M., van den Berg, B., van der Schee, M., de Lange, G., Ellam, R., Govers, R., Gutjahr, M., Hilgen, F., Kouwenhoven, T., Lofi, J., Meijer, P., Sierro, F.J., Bachiri, N., Barhoun, N., Alami, A. C., Chacon, B., Flores, J.A., Gregory, J., Howard, J., Lunt, D., Ochoa, M., Pancost, R., Vincent, S., Yousfi, M.Z., 2015. Evolution of the late Miocene Mediterranean-Atlantic gateways and their impact on regional and global environmental change. Earth Sci. Rev. 150, 365–392.

Fortuin, A.R., Dabrio, C.J., 2008. Evidence for Late Messinian seismites, Nijar Basin, south-east Spain. Sedimentology 55, 1595–1622.

Fortuin, A.R., Krijgsman, W., 2003. The Messinian of the Nijar basin (SE Spain): sedimentation, depositional environments and paleogeographic evolution. Sediment. Geol. 160, 213–242.

Fortuin, A.R., Kelling, J.M.D., Roep, T.B., 1995. The enigmatic Messinian -Pliocene section of Cuevas del Almanzora (Vera Basin, SE Spain) revisited-erosional features and strontium isotope ages. Sediment. Geol. 97, 177–201.

García-Castellanos, D., Micallef, A., Estrada, F., Camerlenghi, A., Ercilla, G., Periáñez, R., Abril, J.M., 2020. The Zanclean megaflood of the Mediterranean–Searching for independent evidence. Earth Sci. Rev. 201 https://doi.org/10.1016/j.earscirev.2019.103061.

García-Veigas, J., Cendón, D.I., Gibert, L., Lowenstein, T.K., Artiaga, D., 2018. Geochemical indicators in Western Mediterranean Messinian evaporites:

implications for the salinity crisis. Mar. Geol. 403, 197–214. https://doi.org/10.1016/j.margeo.2018.06.005.

García-Veigas, J., Gibert, L., Cendon, D.I., Artiaga, D., Corbi, H., Soria, J.M., Lowenstein, T.K., Sanz, E., 2019. Late Miocene evaporite geochemistry of Lorca and Fortuna basins (Eastern Betics, SE Spain): evidences of restriction and continentalization. Basin Res. https://doi.org/10.1111/bre.12408.

Ghielmi, M., Minervini, M., Nini, C., Rogledi, S., Rossi, M., 2013. Late Miocene–Middle Pleistocene sequences in the Po Plain–Northern Adriatic Sea (Italy): the stratigraphic record of modification phases affecting a complex foreland basin. Mar. Pet. Geol. 42, 50–81.

Gliozzi, E., Ceci, M.E., Grossi, F., Ligios, S., 2007. Paratethyan Ostracod immigrants in Italy during the Late Miocene. Geobios 40, 325–337.

Griffin, D.L., 2002. Aridity and humidity: two aspects of the late Miocene climate of North Africa and the Mediterranean. Paleogeogr. Paleoclimatol. Paleoecol. 182 (1–2), 65–91.

Grossi, F., Cosentino, D., Gliozzi, E., 2008. Late Messinian Lago-Mare ostracods and paleoenvironments of the central and eastern Mediterranean Basin. Boll. Soc. Paleontol. Ital. 47 (2), 131–146.

Grossi, F., Gliozzi, E., Anadón, P., Castorina, F., Voltaggio, M., 2015. Is Cyprideis agrigentina Decima a good paleosalinometer for the Messinian Salinity Crisis? Morphometrical and geochemical analyses from the Eraclea Minoa section (Sicily). Paleogeogr. Paleoclimat. Paleoecol. 419, 75–89.

Grothe, A., Sangiorgi, F., Brinkhuis, H., Stoica, M., Krijgsman, W., 2018. Migration of the dinoflagellate Galeacysta etrusca and its implications for the Messinian Salinity Crisis. Newsl. Stratigr. 51 (1), 73–91.

Grothe, A., Andreetto, F., Reichart, G.J., Wolthers, M., Van Baak, C.G., Vasiliev, I., Stoica, M., Sangiorgi, F., Middelburg, J.J., Davies, G.R., Krijgsman, W., 2020. Paratethys pacing of the Messinian Salinity Crisis: low salinity waters contributing to gypsum precipitation? Earth Planet. Sci. Lett. 532, 116029.

Guerra-Merchán, A., Serrano, F., Garcés, M., Gofas, S., Esu, D., Gliozzi, E., Grossi, F., 2010. Messinian Lago-Mare deposits near the strait of Gibraltar (Malaga basin, S Spain). Paleogeogr. Paleoclimat. Paleoecol. 285 (3–4), 264–276.

Gvirtzman, Z., Manzi, V., Calvo, R., Gavrieli, I., Gennari, R., Lugli, S., Reghizzi, M., Roveri, M., 2017. Intra-Messinian truncation surface in the Levant Basin explained by subaqueous dissolution. Geology 45 (10), 915–918.

Hajj, F., Poszwa, A., Bouchez, J., Guérold, F., 2017. Radiogenic and "stable" strontium isotopes in provenance studies: a review and first results on archaeological wood from shipwrecks. J. Archaeol. Sci. 86, 24–49.

Hardie, L.A., Lowenstein, T.K., 2004. Did the Mediterranean Sea dry out during the Miocene? A reassessment of the evaporite evidence from DSDP Legs 13 and 42A cores. J. Sediment. Res. 74, 1–9.

Hart, W., Quade, J., Madsen, D., Kaufman, D., Oviatt, C., 2004. The $^{87}Sr/^{86}Sr$ ratios of lacustrine carbonates and lake-level history of the Bonneville paleolake system. Geol. Soc. Am. Bull. 116 (9), 1107–1119.

Hilgen, F.J., Kuiper, K., Krijgsman, W., Snel, E., Van Der Laan, E., 2007. Astronomical tuning as the basis for high resolution chronostratigraphy: the intricate history of the Messinian salinity crisis. Stratigraphy 4, 231–238.

Hsü, K.J., Ryan, W.B., Cita, M.B., 1973. Late Miocene desiccation of the Mediterranean. Nature 242 (5395), 240–244.

Iaccarino, S., Bossio, A., 1999. Paleoenvironment of uppermost Messinian sequences in the western Mediterranean (Sites 974, 975, and 978). In: Zahn, R., Comas, M.C., Klaus, A. (Eds.), Proc. ODP, Sci. Results, vol. 161. Ocean Drilling Program, College Station, TX, pp. 529–542.

Ingram, B.L., Sloan, D., 1992. Strontium isotopic composition of estuarine sediments as paleosalinity-paleoclimate indicator. Science 255, 68–72.

Jonk, R., Biermann, C., 2002. Deformation in Neogene sediments of the Sorbas and Vera basins (SE Spain): constraints on simpleshear deformation and rigid body rotation along major strike-slip faults. J. Struct. Geol. 24, 963–977.

Karakitsios, V., Roveri, M., Lugli, S., Manzi, V., Gennari, R., Antonarakou, A., Triantaphyllou, M., Agiadi, K., Kontakiotis, G., Kafousia, N., De Rafelis, M., 2017. A record of the Messinian salinity crisis in the eastern Ionian tectonically active domain (Greece, eastern Mediterranean). Basin Res. 29 (2), 203–233.

Kartveit, K.H., Ulsund, H.B., Johansen, S.E., 2019. Evidence of sea level drawdown at the end of the Messinian Salinity Crisis and seismic investigation of the Nahr Menashe Unit in the northern Levant Basin, offshore Lebanon. Basin Res. 31 (5), 827–840.

Keogh, S.M., Butler, R.W.H., 1999. The Mediterranean water body in the late Messinian: interpreting the record from marginal basins on Sicily. J. Geol. Soc. 156 (4), 837–846.

Kirchner, K.L., Behr, W.M., Loewy, S., Stockli, D.F., 2016. Early Miocene subduction in the western Mediterranean: constraints from Rb-Sr multimineral isochron geochronology. Geochem. Geophys. Geosyst. 17 (5), 1842–1860.

Kirkham, C., Bertoni, C., Cartwright, J., Lensky, N.G., Sirota, I., Rodriguez, K., Hodgson, N., 2020. The demise of a 'salt giant' driven by uplift and thermal dissolution. Earth Planet. Sci. Lett. 531, 115933.

Krijgsman, W., Meijer, P.Th., 2008. Depositional environments of the Mediterranean "Lower Evaporites" of the Messinian salinity crisis: constraints from quantitative analyses. Mar. Geol. 253, 73–81.

Krijgsman, W., Garcés, M., Agustí, J., Raffi, I., Taberner, C., Zachariasse, W.J., 2000. The "Tortonian salinity crisis" of the eastern Betics (Spain). Earth Planet. Sci. Lett. 181, 497–511.

Krijgsman, W., Fortuin, A.R., Hilgen, F.J., Sierro, F.J., 2001. Astrochronology for the Messinian Sorbas basin (SE Spain) and orbital (precessional) forcing for evaporite cyclicity. Sediment. Geol. 140, 43–60.

Krijgsman, W., Leewis, M.E., Garcés, M., Kouwenhoven, T.J., Kuiper, K.F., Sierro, F.J., 2006. Tectonic control for evaporite formation in the Eastern Betics (Tortonian; Spain). Sediment. Geol. 188 (189), 155–170.

Krijgsman, W., Stoica, M., Vasiliev, I., Popov, V.V., 2010. Rise and fall of the Paratethys Sea during the Messinian Salinity Crisis. Earth Planet. Sci. Lett. 290 (1–2), 183–191.

Krijgsman, W., Capella, W., Simon, D., Hilgen, F.J., Kouwenhoven, T.J., Meijer, P.T., Sierro, F.J., Tulbure, M.A., van den Berg, B.C.J., van der Schee, M., Flecker, R., 2018. The Gibraltar Corridor: watergate of the Messinian Salinity Crisis. Mar. Geol. 403, 238–246.

Laskar, L.J., Robutel, P., Joutel, F., Gastineau, M., Correia, A.C.M., Levrard, B., 2004. A long term numerical solution for the insolation quantities of thQe Earth. Astron. Astrophys. 428, 261–285.

Lofi, J., Gorini, C., Berne, S., Clauzon, G., dos Reis, A.T., Ryan, W.B.F., Steckler, M.S., 2005. Erosional processes and paleoenvironmental changes in the Western Gulf of Lions (SW France) during the Messinian Salinity Crisis. Mar. Geol. 217, 1–30.

Lu, F.H., 2006. Lithofacies and water-body record of Messinian evaporites in Nijar Basin, SE Spain. Sediment. Geol. 188-189, 115–130.

Lugli, S., Schreiber, B.C., Triberti, B., 1999. Giant polygons in the Realmonte mine (Agrigento, Sicily): evidence for the desiccation of a Messinian halite basin. J. Sediment. Res. 69, 764–771.

Lugli, S., Bassetti, M.A., Manzi, V., Barbieri, M., Longinelli, A., Roveri, M., 2007. The Messinian "Vena del Gesso" evaporites revisited: characterization of isotopic composition and organic matter. Geol. Soc. Spec. Publ. 285, 179–190.

Lugli, S., Roveri, M., Schreiber, C.B., 2010. The Primary Lower Gypsum in the Mediterranean: a new facies interpretation for the first stage of the Messinian salinity crisis. Paleogeogr. Paleoclimat. Paleoecol. 297 (1), 83–99.

Lugli, S., Gennari, R., Gvirtzman, Z., Manzi, V., Roveri, M., Schreiber, B.C., 2013. Evidence of clastic evaporites in the canyons of the Levant Basin (Israel): implications for the Messinian Salinity Crisis. J. Sediment. Res. 83, 942–954.

Lugli, S., Manzi, V., Roveri, M., Schreiber, B.C., 2015. The deep record of the Messinian salinity crisis: evidence of a non-desiccated Mediterranean Sea. Paleogeogr. Paleoclimatol. Paleoecol. 433, 201–218.

Lymer, G., Lofi, J., Gaullier, V., Maillard, A., Thinon, I., Sage, F., Chanier, F., Vendeville, B.C., 2018. The Western Tyrrhenian Sea revisited: new evidence for a rifted basin during the Messinian Salinity Crisis. Mar. Geol. 398, 1–21. https://doi.org/10.1016/j.margeo.2017.12.009.

Madof, A.S., Bertoni, C., Lofi, J., 2019. Discovery of vast fluvial deposits provides evidence for drawdown during the late Miocene Messinian salinity crisis. Geology 47 (2), 171–174.

Maillard, A., Mauffret, A., 2006. Relationship between erosion surfaces and the Late Miocene Salinity Crisis deposits in the Valencia Basin (Northwestern Mediterranean): evidence for an early sea-level drop. Terra Nova 18, 321–329.

Maillard, A., Driussi, O., Lofi, J., Briais, A., Chanier, F., Hübscher, C., Gaullier, V., 2014. Record of the Messinian salinity crisis in the SW Mallorca area (Balearic Promontory, Spain). Mar. Geol. 357, 304–320.

Manzi, V., Lugli, S., Roveri, M., Schreiber, B.C., 2009b. A new facies model for the Upper Gypsum of Sicily (Italy): chronological and paleoenvironmental constraints for the Messinian salinity crisis in the Mediterranean. Sedimentology 56, 1937–1960. https://doi.org/10.1111/j.1365-3091.2009.01063.x.

Manzi, V., Lugli, S., Roveri, M., Dela, Pierre F., Gennari, R., Lozar, F., Natalicchio, M., Schreiber, B.C., Taviani, M., Turco, E., 2016. The Messinian salinity crisis in Cyprus: a further step towards a new stratigraphic framework for Eastern Mediterranean. Basin Res. 28, 207–236.

Manzi, V., Gennari, R., Lugli, S., Persico, D., Reghizzi, M., Roveri, M., Schreiber, B.C., Calvo, R., Gavrieli, I., Gvirtzman, Z., 2018. The onset of the Messinian salinity crisis in the deep Eastern Mediterranean basin. Terra Nova 30 (3), 189–198.

Martín, J.M., Puga-Bernabéu, A., Aguirre, J., Braga, J.C., 2014. Miocene Atlantic-Mediterranean seaways in the Betic Cordillera (Southern Spain). Rev. Soc. Geol. Esp. 27 (1), 175–186.

Martinez-Diaz, J., Hernandez-Enrile, J.N., 2004. Neotectonics and morphotectonics of the southern Almeria region (Betic Cordillera-Spain) kinematic implications. Int. J. Earth Sci. 93, 189–206.

Marzocchi, A., Lunt, D.J., Flecker, R., Bradshaw, C.D., Farnsworth, A., Hilgen, F.J., 2015. Orbital control on late Miocene climate and the North African monsoon: insight from an ensemble of sub-precessional simulations. Clim. Past 11 (10), 1271–1295.

Marzocchi, A., Flecker, R., Van Baak, C.G.C., Lunt, D.J., Krijgsman, W., 2016. Mediterranean outflow pump: an alternative mechanism for the Lago-mare and the end of the Messinian Salinity Crisis. Geology 44, 523–526.

Marzocchi, A., Flecker, R., Lunt, D.J., Krijgsman, W., Hilgen, F.J., 2019. Precessional drivers of late Miocene Mediterranean sedimentary sequences: African summer monsoon and Atlantic winter storm tracks. Paleoceanogr. Paleoclimatol. 34, 1980–1994.

Mather, A.E., Stokes, M., 2001. Marine to continental transition. In: Mather, A.E., Martín, J.M., Harvey, A.M., Braga, J.C. (Eds.), A Field Guide to the Neogene Sedimentary Basins of the Almería Province, SE Spain. Blackwell, Oxford, pp. 1–8.

McArthur, J.M., Howarth, R.J., Shields, G.A., 2012. Strontium isotope stratigraphy. In: Gradstein, F.M., Ogg, J.G., Schmitz, M.D., Ogg, G.M. (Eds.), The Geological Time Scale 2012. Elsevier B.V, Oxford, pp. 127–144.

McCulloch, M.T., De Deckker, P., 1989. Sr isotope constraints on the Mediterranean environment at the end of the Messinian salinity crisis. Nature 342, 62–65.

McKenzie, J.A., Hodell, D.A., Mueller, P.A., Mueller, D.W., 1988. Application of strontium isotopes to late Miocene-early Pliocene stratigraphy. Geology 16 (11), 1022–1025.

Meilijson, A., Hilgen, F., Sepúlveda, J., Steinberg, J., Fairbank, V., Flecker, R., Waldmann, N.D., Spaulding, S.A., Bialik, O.M., Boudinot, F.G., 2019. Chronology with a pinch of salt: integrated stratigraphy of Messinian evaporites in the deep Eastern Mediterranean reveals long-lasting halite deposition during Atlantic connectivity. Earth-Sci. Rev. 194, 374–398. https://doi.org/10.1016/j.earscirev.2019.05.011.

Micallef, A., Camerlenghi, A., García-Castellanos, D., Otero, D.C., Gutscher, M.A., Barreca, G., Spatola, D., Facchin, L., Geletti, R., Krastel, S., Gross, F., Urlaub, M., 2018. Evidence of the Zanclean megaflood in the eastern Mediterranean Basin. Sci. Rep. 8 (1), 1078.

Micallef, A., Camerlenghi, A., Georgiopoulou, A., Garcia-Castellanos, D., Gutscher, M.-A., Lo Iacono, C., Huvenne, V.A.I., Mountjoy, J.J., Paull, C.K., Le Bas, T., Spatola, D., Facchin, L., Accettella, D., 2019. Geomorphic evolution of the Malta Escarpment and implications for the Messinian evaporative drawdown in the eastern Mediterranean Sea. Geomorphology 327, 264–283. https://doi.org/10.1016/j.geomorph.2018.11.012.

Modestou, S., Simon, D., Gutjahr, M., Marzocchi, A., Kouwenhoven, T.J., Ellam, R.M., Flecker, R., 2017. Precessional variability of $^{87}Sr/^{86}Sr$ in the late miocene sorbas basin: an interdisciplinary study of drivers of interbasin exchange. Paleoceanography 32 (6), 531–552.

Montenat, C., Bizon, G., 1976. A propos de l'évolution géodynamique Mio-Pliocène en Méditerranée occidentale. L'example du bassin de Vera (Cordillères béthiques. Espagne méridionale). CR Somm. Soc. Géol. Fr. 1, 15–16.

Montenat, C., Ott d'Estevou, Ph., 1999. The diversity of Late Neogene sedimentary basins generated by wrench faulting in the eastern Betic cordillera, SE Spain. J. Pet. Geol. 22, 61–80.

Mueller, M., Igbokwe, O.A., Walter, B., Pederson, C.L., Riechelmann, S., Richter, D.K., Albert, R., Gerdes, A., Buhl, D., Neuser, R.D., Bertotti, G., Immenhauser, A., 2020. Testing the preservation potential of early diagenetic dolomites as geochemical archives. Sedimentology 67 (2), 849–881. https://doi.org/10.1111/sed.12664.

Müller, D.W., Mueller, P.A., 1991. Origin and age of the Mediterranean Messinian evaporites: Implications from Sr isotopes. Earth Planet. Sci. Lett. 107 (1), 1–12.

Murillo-Barroso, M., Montero-Ruiz, I., Nieto, J.M., Camalich Massieu, M.D., Martín Socas, D., Martinón Torres, M., 2019. Trace elements and lead isotopic composition of copper deposits from the eastern part of the Internal Zone of the Betic Cordillera (SE Iberia): application to provenance of archaeological materials. J. Iber. Geol. 45 (4), 585–608. https://doi.org/10.1007%2Fs41513-019-00111-1.

Nieto, J.M., Puga, E., Díaz de Federico, A., 2000. Late Variscan pyroclastic rocks from the Mulhacén Complex (Betic Cordillera, Spain), 217–24. In: Leyrit, H., Montenat, C. (Eds.), Volcaniclastic Rocks, from Magmas to Sediments. Gordon and Breach Science Publishers, Philadelphia, PA, USA, p. 265.

Omodeo Salé, S., Gennari, R., Lugli, S., Manzi, V., Roveri, M., 2012. Tectonic and climatic control on the Late Messinian sedimentary evolution of the Nijar Basin (Betic Cordillera, Southern Spain). Basin Res. 24, 314–337.

Orszag-Sperber, F., 2006. Changing perspectives in the concept of "Lago-Mare" in Mediterranean Late Miocene evolution. Sediment. Geol. 188, 259–277.

Orszag-Sperber, F., Rouchy, J.M., Blanc-Valleron, M.-M., 2000. La transition Messinien-Pliocène en Méditerranée orientale (Chypre): la période du Lago-Mare et sa signification. C. R. Acad. Sci. Paris, Sci. Terre Planètes 331, 483–490.

Ortí, F., Pérez-López, A., García-Veigas, J., Rosell, L., Céndon, D.I., Pérez-Valera, F., 2014. Sulfate isotope compositions (δ34S, δ18O) and strontium isotopic ratios (87Sr/86Sr) of Triassic evaporites in the Betic Cordillera (SE Spain). Rev. Soc. Geol. Esp. 27 (1), 79–89.

Ott d'Estevou, P., Montenat, C., Alvado, J.C., 1990. Le basin de Vera-Garrucha. In: Montenat, C. (Ed.), Doc. et Trav, vols. 12–13. IGAL, pp. 165–187.

Palmer, M.R., Edmond, J.M., 1992. Controls over the strontium isotope composition of river water. Geochim. Cosmochim. Acta 56 (5), 2099–2111.

Pierre, C., 1982. Teneurs en Isotopes Stables (18O,2H,13C,34S) et Conditions de Génèse des Évaporites Marines: Application à Quelques Milieux Actuels et au Messinien de la Mediterrannée, Ecole Normale Supérieure. Université Paris Sud Orsay, p. 262.

Pierre, C., Fontes, J.-C., 1978. Isotope Composition of Messinian sediments from the Mediterranean Sea as indicators of paleoenvironments and diagenesis. In: Texas A M University, O.D.P.C.S., TX, United States (Ed.), Initial reports of the Deep Sea Drilling, covering Leg 42 of the cruises of the drilling Vessel Glomar Challenger Malaga Spain to Itanbul Turkey. April-May 1975. University of California. Scris Institution of Oceanography, National Science Foundation. National Ocean Sediment Coring Program, pp. 635–650.

Pierre, C., Rouchy, J.M., 1990. Stable isotope composition of carbonates in the Tyrrhenian Sea, Supplement to: Pierre, C; Rouchy, JM (1990): Sedimentary and diagenetic evolution of Messinian evaporites in the Tyrrhenian Sea (ODP Leg 107, Sites 652, 653, and 654): Petrographic, mineralogical, and stable isotope records. In: Kastens, K.A., Mascle, J., et al. (Eds.), Proceedings of the Ocean Drilling Program, Scientific Results, College Station, TX (Ocean Drilling Program), 107, pp. 187–210. https://doi.org/10.2973/odp.proc.sr.107.131.1990. PANGAEA.

Placzek, C.J., Quade, J., Patchett, P.J., 2011. Isotopic tracers of paleohydrologic change in large lakes of the Bolivian Altiplano. Quat. Res. 75 (1), 231–244.

Puga, E., De Federico, A.D., Nieto, J.M., 2002. Tectonostratigraphic subdivision and petrological characterisation of the deepest complexes of the Betic zone: a review. Geodin. Acta 15 (1), 23–43.

Raad, F., Lofi, J., Maillard, A., Tzevahirtzian, A., Caruso, A., 2020. The Messinian Salinity Crisis deposits in the Balearic Promontory: an undeformed analog of the MSC Sicilian basins?? Mar. Pet. Geol. 104777. https://doi.org/10.1016/j.marpetgeo.2020.104777.

Reghizzi, M., Gennari, R., Douville, E., Lugli, S., Manzi, V., Montagna, P., Roveri, M., Sierro, F.J., Taviani, M., 2017. Isotope stratigraphy ($^{87}Sr/^{86}Sr$, δ18O, δ13C) of the Sorbas basin (Betic Cordillera, Spain): paleoceanographic evolution across the onset of the Messinian salinity crisis. Paleogeogr. Paleoclimatol. Paleoecol. 469, 60–73.

Reghizzi, M., Lugli, S., Manzi, V., Rossi, F.P., Roveri, M., 2018. Orbitally forced hydrological balance during the Messinian Salinity Crisis: insights from Strontium Isotopes ($^{87}Sr/^{86}Sr$) in the Vena del Gesso Basin (Northern Apennines, Italy). Paleoceanogr. Paleoclimatol. 33 (7), 716–731.

Ricchiuto, T.E., McKenzie, J.A., 1978. Stable Isotopic investigation of Messinian sulfate samples from DSDP. LEG 42. Eastern Mediterranean Sea. In: Texas A M University, O.D.P.C.S., TX, United States (Ed.), Initial reports of the Deep Sea Drilling covering Leg 42 of the cruises of the drilling vessel Glomar Challenger. Malaga, Spain to Istanbul, Turkey. April-May 1975. University of California. Scripps Institution of Oceanography, National Science Foundation. National Ocen Sediment Coring Program, pp. 657–660.

Roep, Th.B., Van Harten, D., 1979. Sedimentological and ostracodological observations on Messinian post-evaporite deposits in some southeastern Spanish basins. Annales Géologiques des Pays Helleniques 3, 1037–1044.

Roep, Th.B., Dabrio, C.J., Fortuin, A.R., Polo, M.D., 1998. Late highstand patterns of shifting and stepping coastal barriers and washover-fans (late Messinian, Sorbas Basin, SE Spain). Sediment. Geol. 116, 27–56.

Rouchy, J.M., Orszag-Sperber, F., Blanc-Valleron, M.M., Pierre, C., Rivière, M., Combourieu-Nebout, N., Panayides, I., 2001. Paleoenvironmental changes at the Messinian–Pliocene boundary in the eastern Mediterranean (southern Cyprus basins): significance of the Messinian Lago-Mare. Sediment. Geol. 145 (1–2), 93–117.

Roveri, M., Manzi, V., Bassetti, M.A., Merini, M., Ricci Lucchi, F., 1998. Stratigraphy of the Messinian post-evaporitic stage in eastern-Romagna (northern Apennines, Italy). G. Geol. 60, 119–142.

Roveri, M., Bassetti, M.A., Ricci Lucchi, F., 2001. The Mediterranean Messinian salinity crisis: an Apennines foredeep perspective. Sediment. Geol. 140, 201–214.

Roveri, M., Bertini, A., Cosentino, D., Di Stefano, A., Gennari, R., Gliozzi, E., Grossi, F., Iaccarino, S.M., Lugli, S., Manzi, V., Taviani, M., 2008a. A high-resolution stratigraphic framework for the latest Messinian events in the Mediterranean area. Stratigraphy 5 (3–4), 323–342.

Roveri, M., Lugli, S., Manzi, V., Schreiber, B.C., 2008b. The Messinian Sicilian stratigraphy revisited: new insights for the Messinian salinity crisis. Terra Nova 20 (6), 483–488. https://doi.org/10.1111/j.1365-3121.2008.00842.x.

Roveri, M., Gennari, R., Lugli, S., Manzi, V., 2009. The Terminal Carbonate complex: the record of sea-level changes during the Messinian salinity crisis. GeoActa 8 (63), 63–77.

Roveri, M., Flecker, R., Krijgsman, W., Lofi, J., Lugli, S., Manzi, V., Sierro, F.J., Bertini, A., Camerlenghi, A., De Lange, G., Govers, R., Hilgen, F.J., Hübscher, C., Meijer, P.Th., Stoica, M., 2014a. The Messinian salinity crisis: past and future of a great challenge for marine sciences. Mar. Geol. 349, 113–125.

Roveri, M., Lugli, S., Manzi, V., Gennari, R., Schreiber, B.C., 2014b. High resolution strontium isotope stratigraphy of the Messinian deep Mediterranean basins: implications for marginal to central basins correlation. Mar. Geol. 349, 113–125.

Roveri, M., Manzi, V., Bergamasco, A., Falcieri, F.M., Gennari, R., Lugli, S., Schreiber, B. C., 2014c. Dense shelf water cascading and Messinian canyons: a new scenario for the Mediterranean salinity crisis. Am. J. Sci. 314 (3), 751–784. https://doi.org/10.2475/05.2014.03.

Roveri, M., Gennari, R., Persico, D., Rossi, F.P., Lugli, S., Manzi, V., Reghizzi, M., Taviani, M., 2019. A new chronostratigraphic and paleoenvironmental framework for the end of the Messinian salinity crisis in the Sorbas Basin (Betic Cordillera, southern Spain). Geol. J. 54 (3), 1617–1637.

Ruggieri, G., 1967. The Miocene and later evolution of the Mediterranean Sea. In: Adams, Ager (Eds.), Aspects of Tethyan Biogeography, 7. Syst. Ass. Publ, p. 238.

Ryan, W.B., 2009. Decoding the Mediterranean salinity crisis. Sedimentology 56 (1), 95–136.

Sabino, M., Pierre, F.D., Natalicchio, M., Birgel, D., Gier, S., Peckmann, J., 2020. The response of water column and sedimentary environments to the advent of the Messinian salinity crisis: insights from an onshore deep-water section (Govone, NW Italy). Geol. Mag. 1–17.

Sanz de Galdeano, C.S., Santamaría-López, Á., 2019. The lithological sequence of the Nevado-Filábride Complex (Betic Internal Zone) in the sierras Nevada and Filabres. Rev. Soc. Geol. Esp. 32 (1), 113–126.

Sanz de Galdeano, C., Vera, J.A., 1991. Una propuesta de clasificaciòn de las cuencas neógenas beticas. Acta Geol. Hisp. 26, 205–227.

Sanz De Galdeano, C., Vera, J.A., 1992. Stratigraphic record and paleogeographic context of the Neogene basins in the Betic Cordillera, Spain. Basin Res. 4, 21–36.

Schildgen, T.F., Cosentino, D., Frijia, G., Castorina, F., Dudas, F.Ö., Iadanza, A., Sampalmieri, G., Cipollari, P., Caruso, A., Bowring, S.A., Strecker, M.R., 2014. Sea level and climate forcing of the Sr isotope composition of Late Miocene Mediterranean marine basins. Geochem. Geophys. Geosyst. 15, 2964–2983.

Sciuto, F., Baldanza, A., Temani, R., Privitera, G., 2018. New reports of Paratethyan ostracods affinity from the Mediterranean Basin (Sicily, Italy). Paleontol. Electron. 21 (1), 1.

Sierro, F.J., Hilgen, F.J., Krijgsman, W., Flores, J.A., 2001. The Abad composite (SE Spain): a Messinian reference section for the Mediterranean and the APTS. Paleogeogr. Paleoclimatol. Paleoecol. 168, 141–169.

Spatola, D., del Moral-Erencia, J.D., Micallef, A., Camerlenghi, A., Garcia-Castellanos, D., Gupta, S., Bohorquez, P., Gutscher, M.-A., Bertoni, C., 2020. A single-stage megaflood at the termination of the Messinian salinity crisis: geophysical and modelling evidence from the eastern Mediterranean Basin. Mar. Geol. 106337. https://doi.org/10.1016/j.margeo.2020.106337.

Spezzaferri, S., Cita, M.B., McKenzie, J.A., 1998. The Miocene-Pliocene boundary in the Eastern Mediterranean: Results from ODP Leg 160, Sites 967 and 969. In: Robertson, A.H.F., Emeis, K.-C., Richter, C., Camerlenghi, A. (Eds.), Proc. ODP, Sci. Results, vol. 160. Ocean Drilling Program, College Station, TX, pp. 9–28.

Stoica, M., Krijgsman, W., Fortuin, A., Gliozzi, E., 2016. Paratethyan ostracods in the Spanish Lago-Mare: more evidence for intra-basinal exchange at high Mediterranean Sea level. Paleogeogr. Paleoclimatol. Paleoecol. 441, 854–870.

Thinon, I., Guennoc, P., Serrano, O., Maillard, A., Lasseur, E., Rehault, J.P., 2016. Seismic markers of the Messinian Salinity Crisis in an intermediate-depth basin: Data for understanding the Neogene evolution of the Corsica Basin (northern Tyrrhenian Sea). Mar. Pet. Geol. 77, 1274–1296. https://doi.org/10.1016/j.marpetgeo.2016.02.017.

Topper, R.P.M., Flecker, R., Meijer, P.T., Wortel, M.J.R., 2011. A box model of the Late Miocene Mediterranean Sea: implications from combined 87Sr/86Sr and salinity data. Paleoceanography 26, PA3223.

Topper, R.P.M., Lugli, S., Manzi, V., Roveri, M., Meijer, P.T., 2014. Precessional control of Sr ratios in marginal basins during the Messinian salinity crisis? Geochem. Geophys. Geosyst. 15-5, 1926–1944.

Toscani, L., Venturelli, G., Barbieri, M., Capedri, S., Soler, J.F., Oddone, M., 1990. Geochemistry and petrogenesis of two-pyroxene andesites from Sierra de Gata (SE Spain). Mineral. Petrol. 41 (2–4), 199–213.

Van Baak, C.G.C., Stoica, M., Grothe, A., Aliyeva, E., Krijgsman, W., 2016. Mediterranean-Paratethys connectivity during the Messinian salinity crisis: the Pontian of Azerbaijan. Glob. Planet. Chang. 141, 63–81.

van de Poel, H.M., 1991. Messinian stratigraphy of the Nijar Basin (S.E. Spain) and the origin of its gypsum-ghost limestones. Geol. Mijnb. 70, 215–234.

Vasiliev, I., Reichart, G.-J., Davies, G.R., Krijgsman, W., Stoica, M., 2010. Strontium isotope ratios of the Eastern Paratethys during the Mio-Pliocene transition; Implications for interbasinal connectivity. Earth Planet. Sci. Lett. 292, 123–131.

Vasiliev, I., Mezger, E.M., Lugli, S., Reichart, G.J., Manzi, V., Roveri, M., 2017. How dry was the Mediterranean during the Messinian salinity crisis? Paleogeogr. Paleoclimatol. Paleoecol. 471, 120–133.

Veizer, J., 1989. Strontium isotopes in seawater through time. Annu. Rev. Earth Planet. Sci. 17 (1), 141–167.

Vera, J.A., 2000. El terciario de la Cordillera Bética: estado actual de conocimientos. Rev. Soc. Geol. Esp. 13, 345–373.

Vera, J.A., 2001. Evolution of the South Iberian continental margin. In: Ziegler, P.A., Cavazza, W., Robertson, A.H.F., Crasquin-Soleau, S. (Eds.), Peri-Tethys Memoir 6: Peri-Tethyian Rift/Wrench Basins and Passive Margins, 186. Mem. Mus. Natn. Hist. Nat, pp. 109–143.

Völk, H.R., Rondeel, H.E., 1964. Zur Gliedenmg des Jungtertilrs im Becken von Vera. Stidostspanien. Geol. Mijnb. 43, 310–315.

Vonhof, H.B., Wesselingh, F.P., Ganssen, G.M., 1998. Reconstruction of the Miocene western Amazonian aquatic system using molluscan isotopic signatures. Paleogeogr. Paleoclimatol. Paleoecol. 141, 85–93.

Zeck, H.P., Kristensen, A.B., Williams, I.S., 1998. Post-collisional volcanism in a sinking slab setting-crustal anatectic origin of pyroxene-andesite magma, Caldear Volcanic Group, Neogene Alborán volcanic Province, southeastern Spain. Lithos 45 (1–4), 499–522.

Zielinski, M., Dopieralska, J., Belka, Z., Walczak, A., Siepak, M., Jakubowicz, M., 2017. The strontium isotope budget of the Warta River (Poland): between silicate and carbonate weathering, and anthropogenic pressure. Appl. Geochem. 81, 1–11.